

ENCLOSURE 2

CORRECTED DOCUMENTATION FOR RELIEF REQUEST NUMBER RR 4-18

Discussion

Entergy Nuclear Operations, Inc., (ENO) submitted a proposed alternative (relief request number RR 4-18) concerning volumetric examinations of the subject branch connection welds on February 25, 2014 (Reference 1), and supplemental information was submitted on March 1, March 4, March 6, March 9, and March 11, 2014 (References 2 through 7).

On March 12, 2014 (Reference 8), the NRC staff verbally authorized the use of relief request number RR 4-18 at PNP until the next scheduled refueling outage, scheduled in the fall of 2015 (1R24). A NRC safety evaluation detailing the technical basis for the verbal authorization was subsequently issued on September 4, 2014 (Reference 9). The safety evaluation credited the ENO flaw and structural evaluation, in addition to the identified hardship and conditions of relief identified in the proposed alternative, in concluding that ENO had provided sufficient information to demonstrate reasonable assurance of the structural integrity of the nine subject welds for one cycle of operation without performing a volumetric examination.

On February 27, 2015, Structural Integrity Associates, Inc. (SI) verbally notified ENO of a discrepancy discovered in the residual stress calculation (Calculation No. 1200895.306) that was submitted on March 6, 2014 (Reference 4). In a letter to ENO dated March 6, 2015, SI stated that the discrepancy was discovered in the load application for the normal operating conditions (NOC) evaluation. Specifically, the inside diameter surface elements adjacent to the circumferential free end and the axial free end of the hot leg pipe did not receive pressure loading (i.e., the effective pressure was 0 psig), while the remaining internal surfaces were pressurized to 2,122 psig for the NOC cycles.

The pressure application for the hydrostatic test condition in the calculation was also reviewed, and the same pressure discrepancy was discovered. However, the application and subsequent removal of the erroneous hydrostatic test pressure loading did not significantly affect the residual stress condition at 70°F, indicating that applied pressure did not generate significant yield level stresses in the weld region.

In the case of the NOC evaluation, the stresses generated during the loaded state were used in subsequent calculations for crack growth life determination. Therefore, it was necessary to understand how the erroneous pressure application altered the stress results in the loaded condition. The erroneously applied pressure caused an unbalanced pressure load, which introduced a bending moment into the hot leg pipe wall rather than an expected radial and axial expansion typical of internally applied pressure in the piping. In particular, the induced moment tended to create a compressive (i.e., less tensile) stress behavior in and around the inside of the nozzle-to-pipe weld. As a result, the erroneously applied pressure reduced the radial and hoop tensile stresses at the weld inside diameter rather than increase them.

ENCLOSURE 2

The SI calculations were revised to correct the discrepancy and the associated SI reports were updated to reflect the updated calculations. The revised SI calculations and updated memorandums are provided in the attachment.

The revised calculations and updated reports are provided for informational purposes only and do not provide the technical basis for the proposed alternative described in Enclosure 1.

References

1. Entergy Nuclear Operations, Inc. letter PNP 2014-015, "Relief Request Number RR 4-18 Proposed Alternative, Use of Alternate ASME Code Case N-770-1 Baseline Examination," dated February 25, 2014 (ADAMS Accession No. ML14056A533).
2. Entergy Nuclear Operations, Inc. letter PNP 2014-021, "Response to Request for Additional Information dated February 26, 2014, for Relief Request Number RR 4-18 – Proposed Alternative, Use of Alternate ASME Code Case N-770-1 Baseline Examination," dated March 1, 2014 (ADAMS Accession No. ML14072A361).
3. Entergy Nuclear Operations, Inc. letter PNP 2014-022, "Response to Second Request for Additional Information dated February 27, 2014, for Relief Request Number RR 4-18 – Proposed Alternative, Use of Alternate ASME Code Case N-770-1 Baseline Examination," dated March 4, 2014 (ADAMS Accession No. ML14063A089).
4. Entergy Nuclear Operations, Inc. letter PNP 2014-028, "Supplemental Response to Request for Additional Information dated February 26, 2014, for Relief Request Number RR 4-18 – Proposed Alternative, Use of Alternate ASME Code Case N-770-1 Baseline Examination," dated March 6, 2014 (ADAMS Accession No. ML14066A409).
5. Entergy Nuclear Operations, Inc. letter PNP 2014-029, "Response to Third Request for Additional Information dated March 5, 2014, for Relief Request Number RR 4-18 – Proposed Alternative, Use of Alternate ASME Code Case N-770-1 Baseline Examination," dated March 6, 2014 (ADAMS Accession No. ML14070A182).
6. Entergy Nuclear Operations, Inc. letter PNP 2014-030, "Second Supplemental Response to Request for Additional Information dated February 26, 2014, for Relief Request Number RR 4-18 – Proposed Alternative, Use of Alternate ASME Code Case N-770-1 Baseline Examination," dated March 9, 2014 (ADAMS Accession No. ML14069A004).
7. Entergy Nuclear Operations, Inc. letter PNP 2014-031, "Response to Fourth Request for Additional Information dated March 11, 2014, for Relief Request Number RR 4-18 – Proposed Alternative, Use of Alternate ASME Code Case N-770-1 Baseline Examination," dated March 11, 2014 (ADAMS Accession No. ML14070A477).

ENCLOSURE 2

8. NRC Electronic Mail, "Palisades Nuclear Plant – Verbal Authorization for Relief Request RR 4-18 - MF3508," March 13, 2014 (ADAMS Accession No. ML14073A274).
9. NRC letter, "Palisades Nuclear Plant – Proposed Alternative, Use of Alternate ASME Code Case N-770-1 Baseline Examination (TAC No. MF3508)," dated September 4, 2014 (ADAMS Accession No. ML142238226).

ENCLOSURE 2 ATTACHMENT

The attached Structural Integrity Associates, Inc. reports and calculations are provided for informational purposes only and do not provide the technical basis for the enclosed proposed alternative.

1. Structural Integrity Associates, Inc., Letter Report No. 1400669.403.R0, "Evaluation of the Palisades Nuclear Plant Hot Leg Drain Nozzle for Primary Water Stress Corrosion Cracking," Revision 0, dated May 8, 2015.
2. Structural Integrity Associates, Inc., Letter Report No. 1400669.404.R0, "Additional Evaluations of the Palisades Nuclear Plant Hot Leg Drain Nozzle for Primary Water Stress Corrosion Cracking," Revision 0, dated May 8, 2015.
3. Structural Integrity Associates, Inc., Calculation 1200895.306, "Hot Leg Drain Nozzle Weld Residual Stress Analysis and Circumferential Crack Stress Intensity Factor Determination," Revision 1, dated May 8, 2015.
4. Structural Integrity Associates, Inc., Calculation 1200895.307, "Hot Leg Drain Nozzle Crack Growth Analyses," Revision 1, May 8, 2015.
5. Structural Integrity Associates, Inc., Calculation 1200895.308, "Hot Leg Drain Nozzle Limit Load Analyses for Flawed Nozzle-to-Hot Leg Weld," Revision 1, dated May 8, 2015.



5215 Hellyer Ave.
Suite 210
San Jose, CA 95138-1025
Phone: 408-978-8200
Fax: 408-978-8964
www.structint.com
rmattson@structint.com

May 8, 2015

Report No. 1400669.403.R0

Quality Program: ☒ Nuclear ☐ Commercial

William Sims
Director, Chief Engineer
Major Projects
1448 S.R. 333
Russellville, Arkansas
72802

Subject: Evaluation of the Palisades Nuclear Plant Hot Leg Drain Nozzle for Primary Water Stress Corrosion Cracking

- References:
- 1) Structural Integrity Associates Memorandum RAM-14-008, "Evaluation of the Palisades Nuclear Plant Hot Leg Drain Nozzle for Primary Water Stress Corrosion Cracking," dated February 25, 2014, SI File No. 1200895.408.
 - 2) ANSYS Mechanical APDL and PrepPost, Release 14.5 (w/ Service Pack 1), ANSYS, Inc., September 2012.
 - 3) Structural Integrity Associates Calculation No. 1200895.306, Revision 1, "Hot Leg Drain Nozzle Weld Residual Stress Analysis and Circumferential Crack Stress Intensity Factor Determination."
 - 4) Letter from G. White (Dominion Engineering, Inc.) to W. Sims (Entergy), "Effect of Post-Weld Heat Treatment Applied to Alloy 82/182 Full-Penetration Branch Pipe Connection Welds at Palisades," L-4199-00-01, Rev. 0, dated February 25, 2014, SI File No. 1200895.408.
 - 5) Structural Integrity Associates Calculation No. 1200895.307, Revision 1, "Hot Leg Drain Nozzle Crack Growth Analyses."
 - 6) *Materials Reliability Program: Crack Growth Rates for Evaluating Primary Water Stress Corrosion Cracking (PWSCC) of Alloy 82, 182 and 132 Welds (MRP-115)*, EPRI, Palo Alto, CA: 2004, 1006696.
 - 7) Structural Integrity Associates Calculation No. 1200895.308, Revision 1, "Hot Leg Drain Nozzle Limit Load Analyses for Flawed Nozzle-to-Hot Leg Weld."
 - 8) ASME Boiler and Pressure Vessel Code, Section III, *Rules for Construction of Nuclear Facility Components*, 2001 Edition with Addenda through 2003.
 - 9) ASME Boiler and Pressure Vessel Code, Section XI, *Rules for Inservice Inspection of Nuclear Plant Components*, 2001 Edition with Addenda through 2003.

Toll-Free 877-474-7693

Chicago, IL
877-474-7693

Akron, OH
330-899-9753
Denver, CO
303-792-0077

Austin, TX
512-533-9191
San Diego, CA
858-455-6350

Charlotte, NC
704-597-5554
San Jose, CA
408-978-8200

Chattanooga, TN
423-553-1180
State College, PA
814-954-7776

Toronto, Canada
905-829-9817

Dear William,

Structural Integrity Associates has been contracted by Entergy to evaluate the Alloy 82/182 full penetration weld which connects the hot leg to the drain nozzle. The evaluation focuses on the probability of occurrence of primary water stress corrosion cracking (PWSCC), and the PWSCC growth of a postulated axial and circumferential flaw in the weld.

The original Memorandum, RAM-14-008 [1], has been revised and reissued as a Letter Report to incorporate new circumferential and axial crack growth evaluations that were developed due to an error in an earlier weld residual stress analysis, which generated an inaccurate residual stress field and resulted in un-conservative crack growth durations.

Finite Element Analyses

A three-dimensional finite element model encompassing 90° of the circumference was constructed using the ANSYS software [2]. Per Reference 3, the weld was modeled with eighty-seven nuggets representing the lumped weld beads connecting the hot leg to the nozzle. Figure 1 depicts the finite element model, and Figures 2 and 3 depict the weld and patch nuggets, respectively.

Analyses were performed for the following steps of construction:

1. Deposit cladding on hot leg inside surface (ID).
2. Install drain line nozzle/backing ring and deposit weld.
3. Remove backing ring and deposit ID patch.
4. Post weld heat treatment, including creep effects based upon experimental data.
5. Subject the configuration to a hydrostatic test.
6. Impose five cycles of "shake down" at normal operating temperature and pressure.

Stress results normal to a circumferential crack are shown in Figure 4, and those normal to an axial crack are shown in Figure 5.

Crack tip elements along the nozzle-weld boundary were evaluated at seven depths through the thickness, and at 0°, 30°, 60° and 90° angular locations, for a postulated circumferential flaw. A plot of the applied stress intensity vs. crack depth is shown in Figure 6 for the circumferential flaw.

Assessment of Likelihood of PWSCC Initiation

The likelihood of PWSCC initiation occurring on the wetted Alloy 600 and Alloy 82/182 surfaces of the Palisades hot leg drain nozzle was assessed by Dominion Engineering, Inc. (DEI) [4]. This assessment concludes that there is a low probability that a stress corrosion crack of engineering size has initiated in the Alloy 82/182 full penetration branch pipe connection welds at Palisades, including in the hot leg drain nozzle and full penetration weld. The low probability of initiation is the result of the nickel-based material being exposed to the post weld heat treatment (PWHT) applied to the adjacent carbon steel material. The greatly reduced

susceptibility to the occurrence of PWSCC of Alloy 600 weldments that have been exposed to PWHT after welding is demonstrated by the following:

- Detailed laboratory investigations including studies that show a very significant relaxation of the residual stress in the surface layer of the weldment,
- PWR plant experience showing hundreds of cases of PWSCC when the Alloy 82/182 or Alloy 600 material was not exposed to PWHT, but extremely few cases when the material was exposed to PWHT subsequent to welding, and,
- the favorable operating temperatures of the Alloy 600 branch connection nozzles at Palisades (eight operate at the relatively low reactor cold leg temperature, and only the single hot leg drain nozzle operates at reactor hot leg temperature).

The finite element analyses [3] for the hot leg drain nozzle showed peak total tensile stresses on the wetted surface for normal operating conditions of 16 to 36 ksi. As discussed in the DEI letter, given the large demonstrated sensitivity of initiation time to surface stress, there is a low probability that PWSCC initiation of a flaw of engineering size has occurred on this weldment at Palisades. Because of the cold leg operating temperature of the nozzles located on the Palisades cold legs, and because the weld residual stress is expected to be similar for the cold leg locations, this conclusion extends to the eight cold leg nozzles.

Crack Growth Evaluation

Growth of circumferential and axial flaws was investigated in Reference 5 in order to assess the consequences of such hypothetical cracking in the case of PWSCC initiation. Using the applied stress intensity factors described above for a circumferential flaw, crack growth through the depth of the weld was calculated, and the results are presented in Figure 7 for the circumferential flaw. For the axial flaw, a conservative classical fracture mechanics solution was used for an elliptical flaw which has a constant width along the inside surface of the Alloy 600 nozzle and Alloy 82/182 weld, and a variable depth through the thickness. Three widths for the elliptical flaw were modeled. Figures 8 and 9 present the applied stress intensity factors vs. crack depth and crack growth for the axial flaw, respectively. However, more realistic, less conservative results can be obtained using finite element analysis techniques for the axial flaw as was done for the circumferential flaw. The crack growth law used in developing these plots is as described in MRP-115 [6].

As discussed in the DEI letter, laboratory crack growth testing has shown a significant benefit of PWHT in reducing the crack growth rate for Alloy 182 weld metal (e.g., by a factor of between two and four). This benefit is conservatively not credited in the MRP-115 crack growth rate equation for Alloy 182.

Limit Analysis

Circumferential Cracking:

In the event that circumferential PWSCC were to occur in the Alloy 82/182 full penetration weld, the variability in residual stress with azimuthal position around the nozzle (for the geometry of a nozzle welded into a cylindrical pipe) would tend to drive crack growth through-wall along part of the circumference. This non-axisymmetric crack growth behavior would be expected ultimately to result in detection of leakage prior to the possibility of unstable pipe rupture.

At 40 effective full power years, the finite element model described above was modified in Reference 7 to include "cracking" at the four circumferential locations documented in Table 3 of Reference 5. This flaw is predicted to be through-wall for 35° in each 90° of arc (70° for each 180° of the circumference in the final model) using the MRP-115 crack growth rate equation [6]. The hypothetical partial-arc through-wall circumferential flaw is illustrated in Figure 10. A limit analysis, as described in ASME Code, Section III, Subparagraph NB-3228.1 [8], was performed, taking into consideration the effects of the flux Alloy 82/182 weld by decreasing the weld metal effective yield strength by the "Z" factor [9, Appendix C, C-6330]. The limit analysis results satisfy the Section III criteria. The analysis, which applied Level A Service Limits of the ASME Code, showed that the flaw remains stable at 1.71 times the applied loads.

Axial Cracking:

For the axial flaw, the flaw modeled in ANSYS was initially assumed to be at a depth of 75% through-wall. The analysis satisfies the ASME Code, Section III criteria [8]. Per Figure 9, this equates to 11.3 effective full power years of operation, assuming a 2" wide axial flaw. As noted above, if more detailed finite element analyses were performed, there would be an increase in the effective full power years of operation corresponding to a flaw depth of 75% through-wall.

Another limit analysis was performed in order to investigate the stability of a hypothetical axial flaw that has grown through-wall to encompass the entire Alloy 82/182 weld cross-section and a large portion of the Alloy 600 nozzle. The extent of this conservatively assumed axial flaw is shown in Figure 11. The analysis, which applied Level A Service Limits of the ASME Code, showed that the flaw remains stable at 1.87 times the applied loads. This limit analysis shows that the structural stability provided by the pipe branch connection geometry would be expected to preclude the possibility of a rupture. Leakage and not rupture would be the ultimate result of growth of an axial flaw.

Conclusions

Based on the assessments and calculations performed, it is concluded that the visual examinations for evidence of pressure boundary leakage required by ASME Code Case N-722-1 are sufficient to ensure that nuclear safety is maintained (i.e., periodic volumetric/surface examinations for indications of PWSCC are not necessary). The adequacy of visual examinations to address the PWSCC concern is demonstrated by the following:

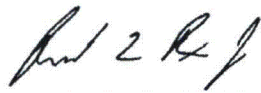
- Because of the PWHT of the nickel-based materials, there is a low probability that a stress corrosion crack of engineering size has initiated on the Alloy 82/182 full penetration branch pipe connection welds at Palisades. Confidence in this conclusion is provided by a combination of laboratory investigations, extensive plant experience, the favorable operating temperatures, and finite element weld residual stress analyses specific to Palisades.
- In the unlikely case that crack initiation were to occur, crack growth calculations considering PWSCC as the failure mechanism demonstrate that the hot leg drain nozzle weldment satisfies ASME Code acceptance criteria (i.e., 75% through-wall) for 20 effective full power years for a circumferential flaw, and 11.3 years for an axial flaw. These results are highly conservative in that they assume a crack could initiate, that a crack initiates immediately at the start of plant operation, and that a conservative limit load analysis is satisfied. In the unlikely case that a crack has already initiated, it would most likely have occurred closer in time to today than to plant startup.
- The ultimate result of any circumferential or axial cracking would very likely be detection of leakage prior to the possibility of unstable pipe rupture. In the unlikely case of initiation of an axial crack and the unlikely case that an axial crack were to exceed a depth of 75% through-wall, the structural stability provided by the pipe branch connection geometry would be expected to preclude the possibility of a rupture. Leakage and not rupture would be the ultimate result of growth of an axial flaw. Similarly, in the unlikely case of initiation of a circumferential crack and the unlikely case that a circumferential crack were to exceed a depth of 75% through-wall, non-axisymmetric crack growth behavior would be expected ultimately to result in detection of leakage prior to the possibility of unstable pipe rupture. The periodic visual examinations for evidence of leakage that are performed during every refueling outage for the hot leg drain nozzle per ASME Code Case N-722-1 are direct examinations of the metal surface that are capable of detecting small amounts of pressure boundary leakage.

Finally, the potential presence of weld repairs made during plant construction would not affect these conclusions. Any such weld repairs would have been made prior to PHWT being applied, and would be expected to extend over a relatively limited circumferential portion of the original weld. The PWHT would relax the residual stresses in the weld repair area, including the substantial relaxation expected at the surface exposed to primary coolant. Moreover, in the unlikely case that initiation occurred in the area of a weld repair, the weld repair would be an additional source of non-axisymmetric crack loading that would tend to drive crack growth through-wall over a relatively local circumferential region, ultimately resulting in detection of leakage prior to the possibility of unstable pipe rupture.

Evaluation of the Palisades Nuclear Plant Hot Leg Drain Nozzle for Primary Water Stress
Corrosion Cracking

These conclusions extend to the pipe connection Alloy 82/182 full penetration weldments on the reactor cold legs at Palisades. The assessments presented above for the single hot leg location clearly bound the concern for PWSCC at each of the cold leg locations. The susceptibility to PWSCC initiation is greatly reduced for nickel-based weldments operating at reactor cold leg temperature, and the PWSCC growth rate at reactor cold leg temperature is approximately four times lower than the corresponding crack growth rate at reactor hot leg temperature (considering the standard thermal activation energy for crack growth of 130 kJ/mole per MRP-115 [6]). The PWHT applied to the cold leg locations is expected to result in similar residual stress levels as those calculated for the hot leg drain nozzle.

Prepared by:

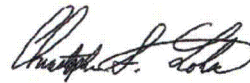


Richard Bax
Associate

5/8/2015

Date

Verified by:



Chris Lohse
Senior Consultant, P.E.

5/8/2015

Date

Approved by:



Richard Mattson
Senior Associate, P.E.

5/8/2015

Date

cc: Norman Eng
Christine King

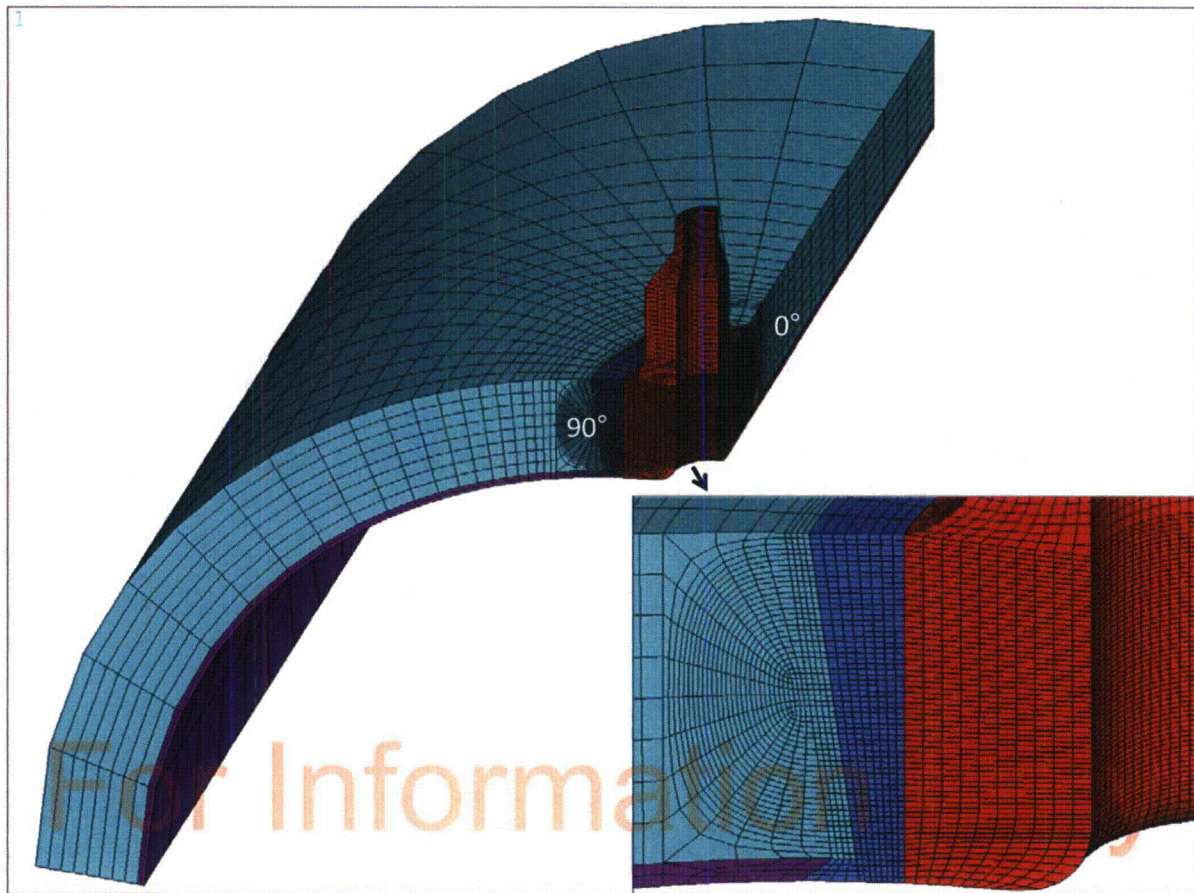


Figure 1. Finite Element Model

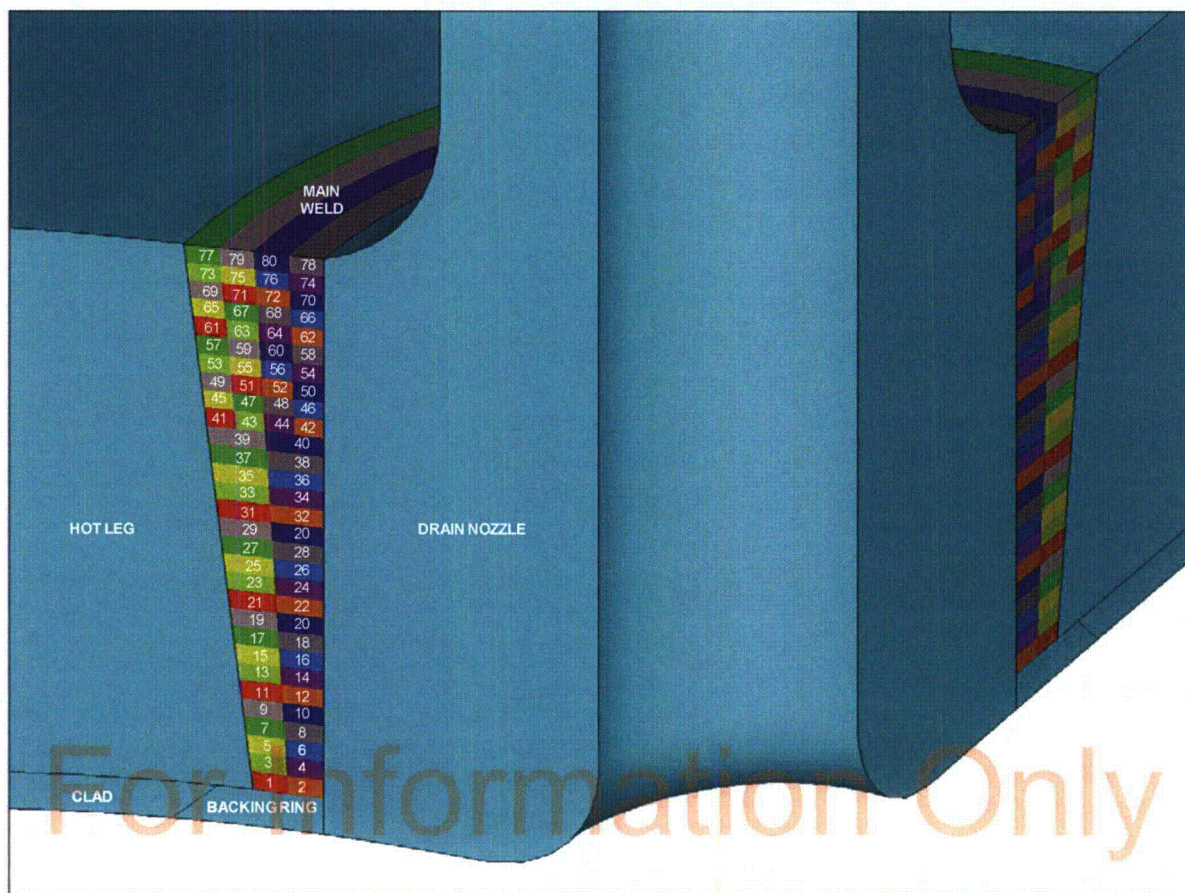


Figure 2. Weld Nuggets

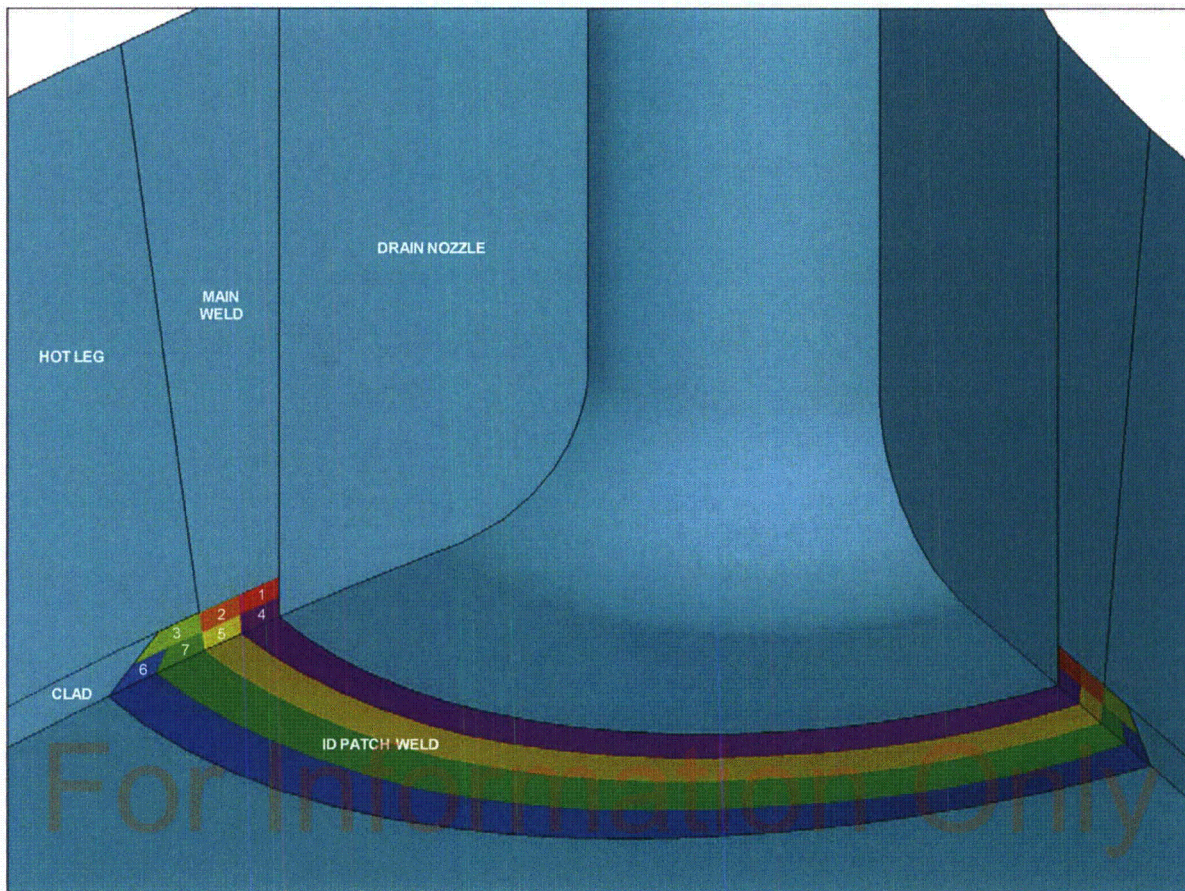


Figure 3. Patch Nuggets

Evaluation of the Palisades Nuclear Plant Hot Leg Drain Nozzle for Primary Water Stress
Corrosion Cracking

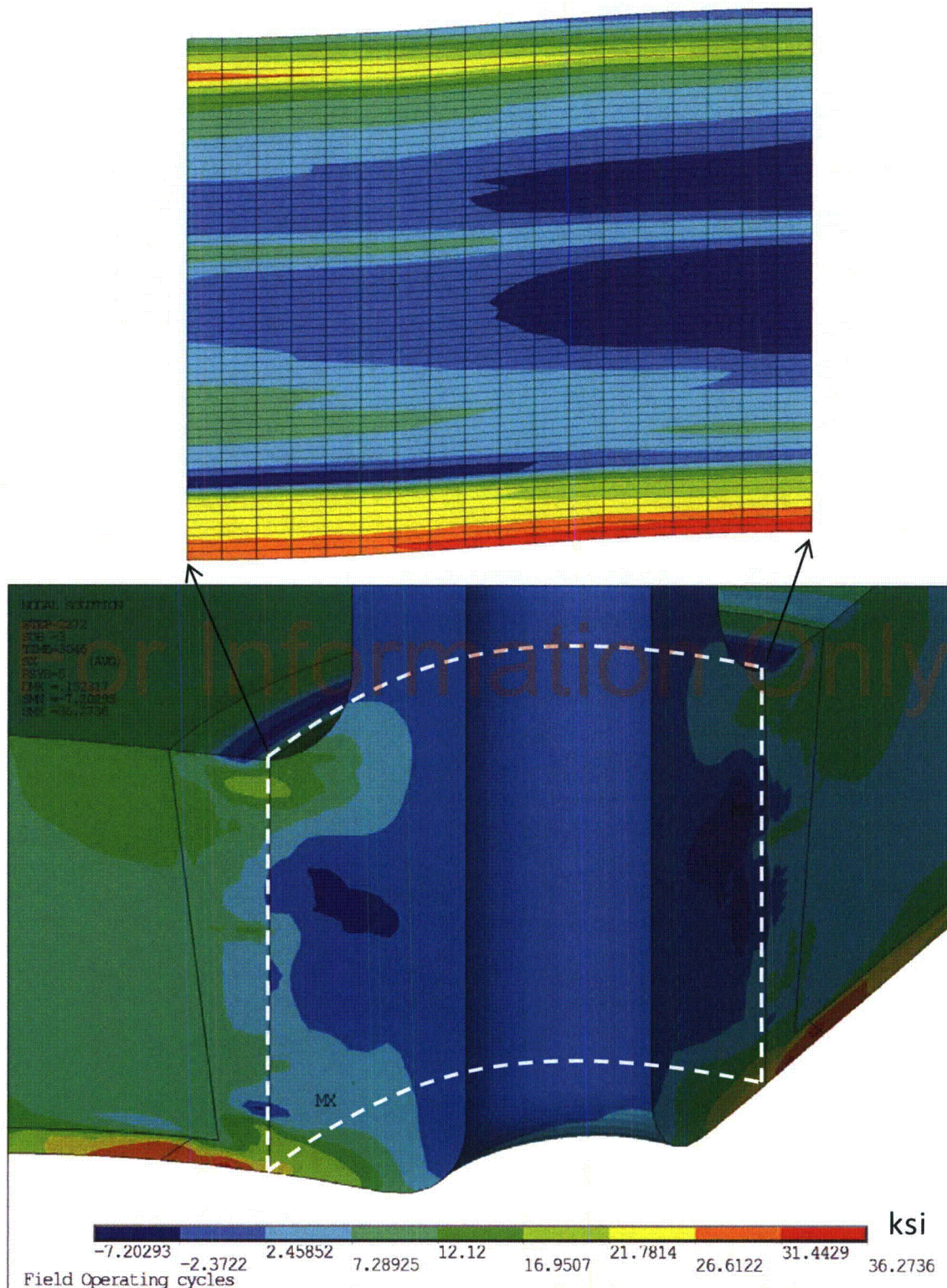


Figure 4. Radial Stresses at Operating Conditions

Evaluation of the Palisades Nuclear Plant Hot Leg Drain Nozzle for Primary Water Stress
Corrosion Cracking

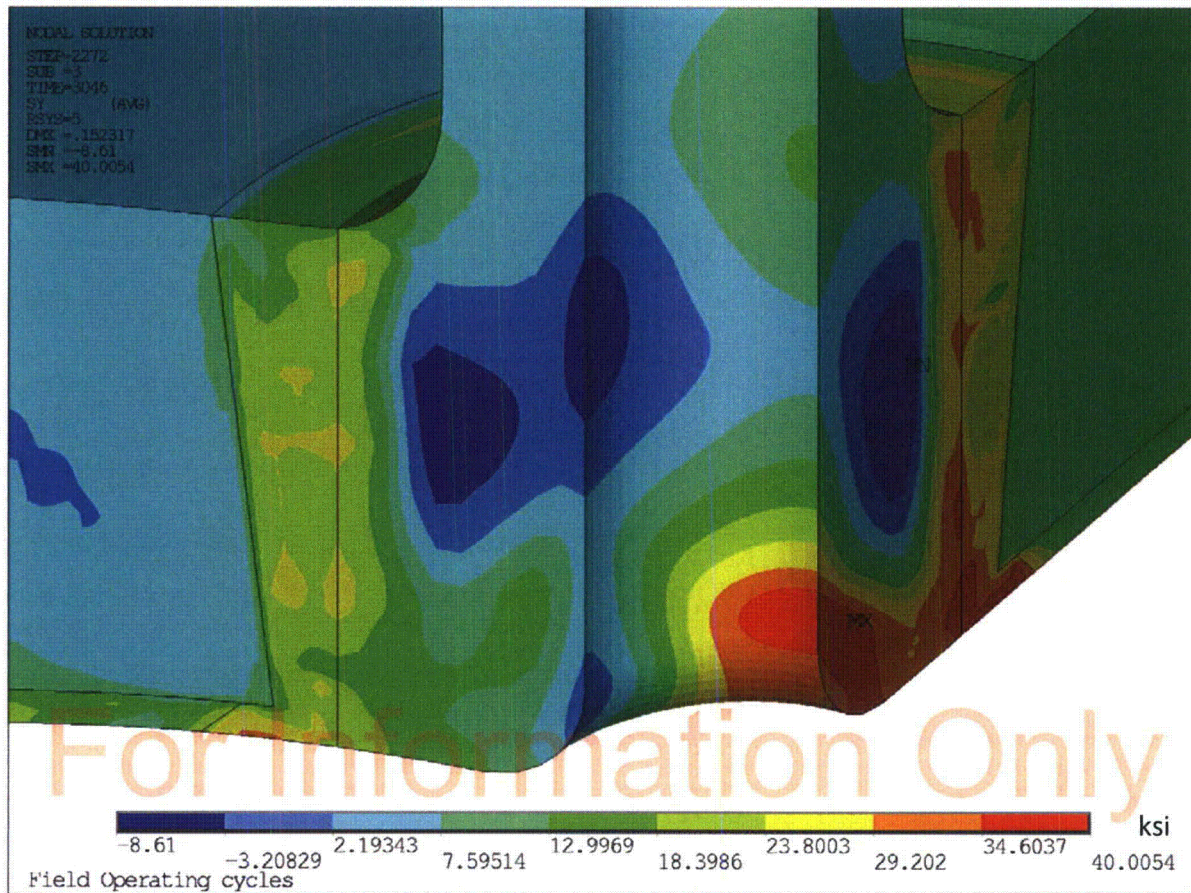


Figure 5. Circumferential Stresses at Operating Conditions

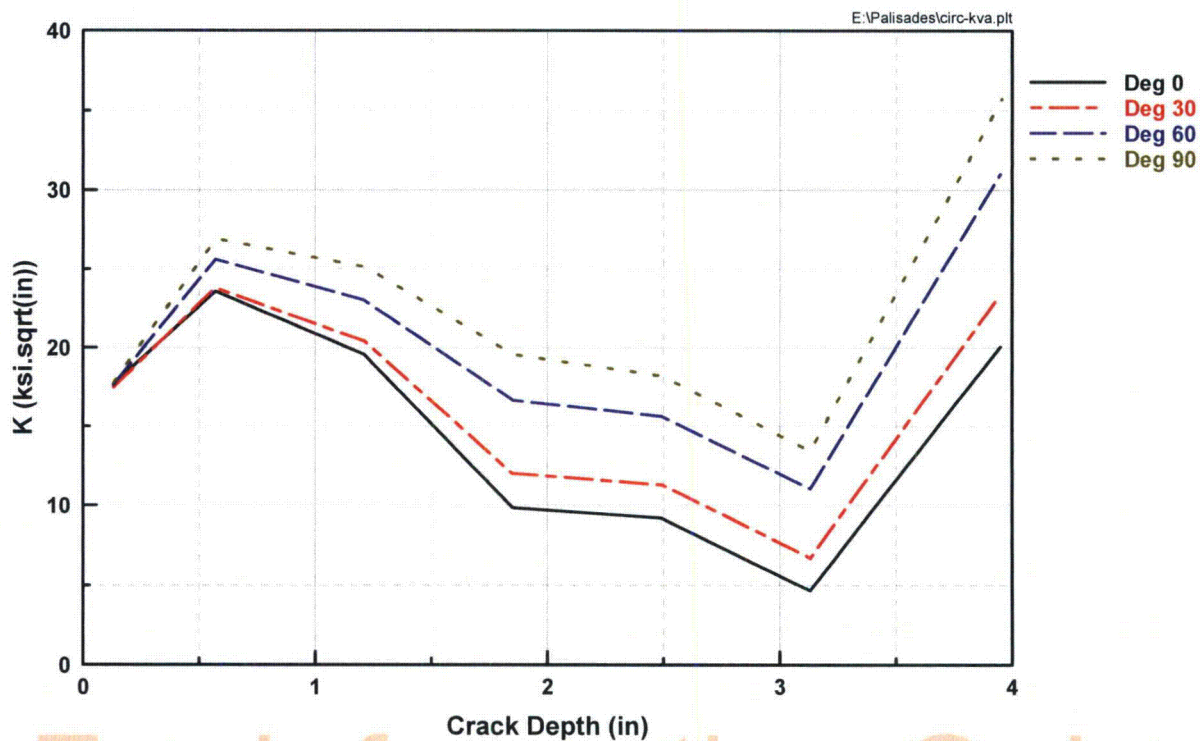


Figure 6. Applied Stress Intensity Factor vs. Crack Depth – Circumferential Flaw

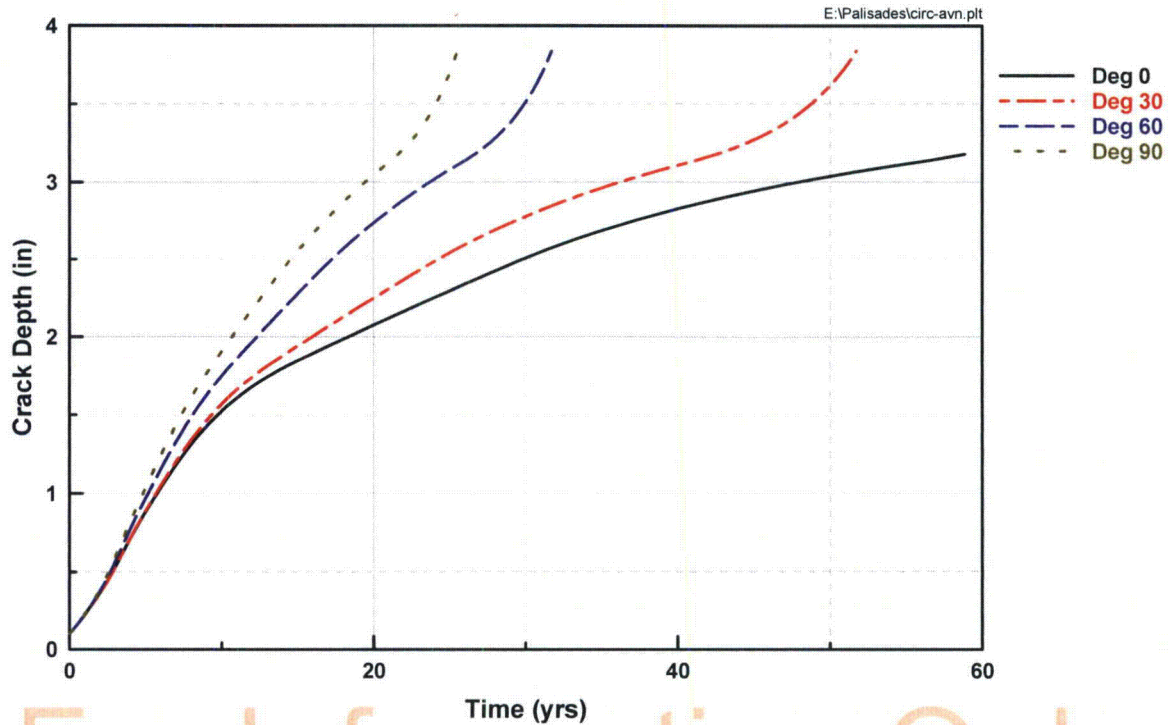


Figure 7. Crack Growth for Circumferential Flaw

Note: Wall Thickness is 4".

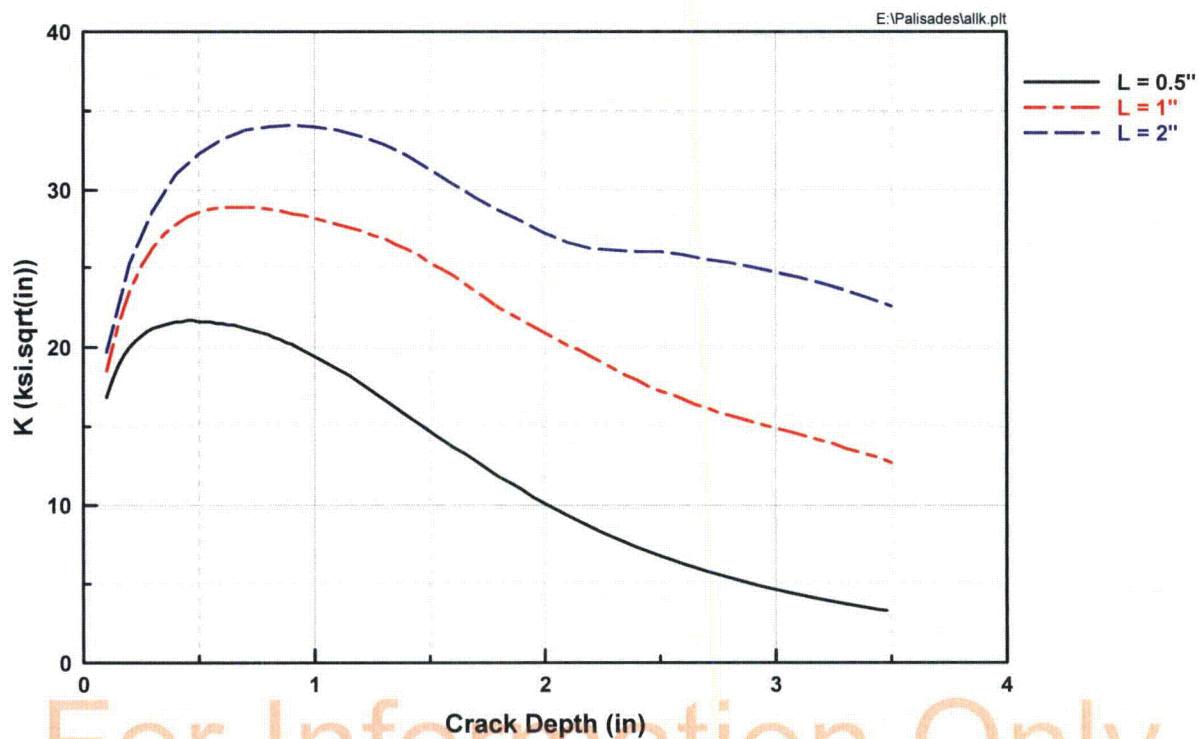


Figure 8. Applied Stress Intensity Factor vs. Crack Depth – Axial Flaw

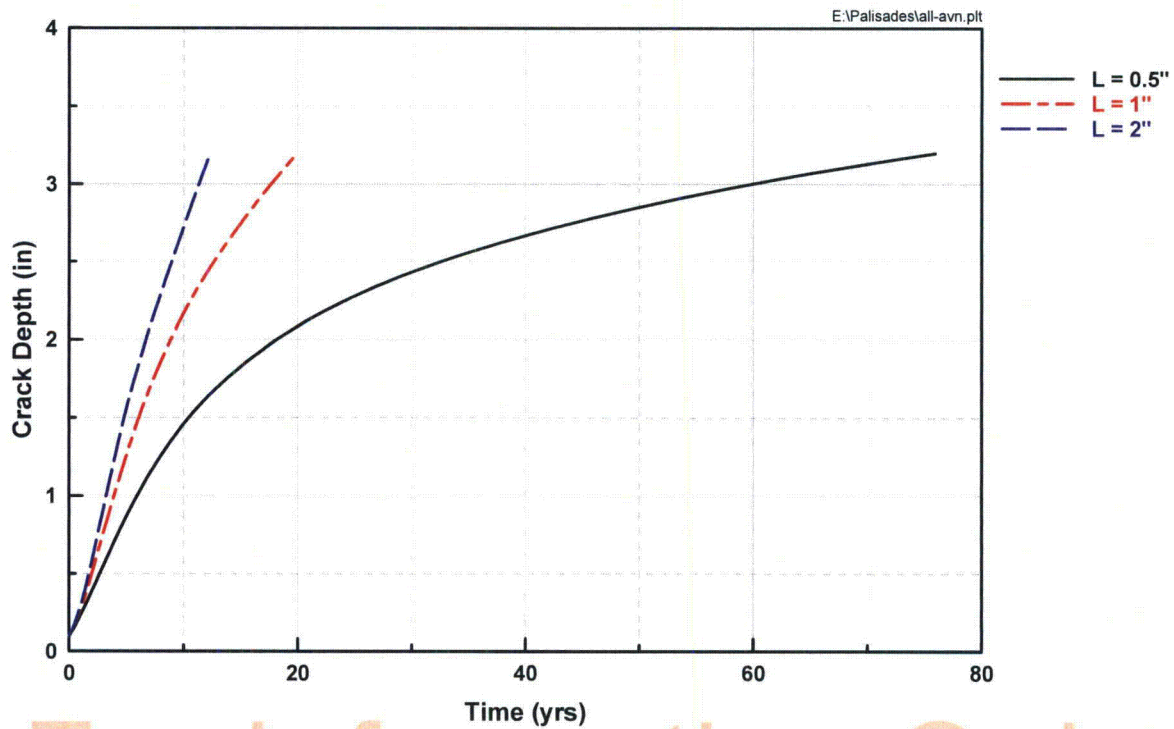


Figure 9. Crack Growth for Axial Flaw

Note: Wall Thickness is 4".

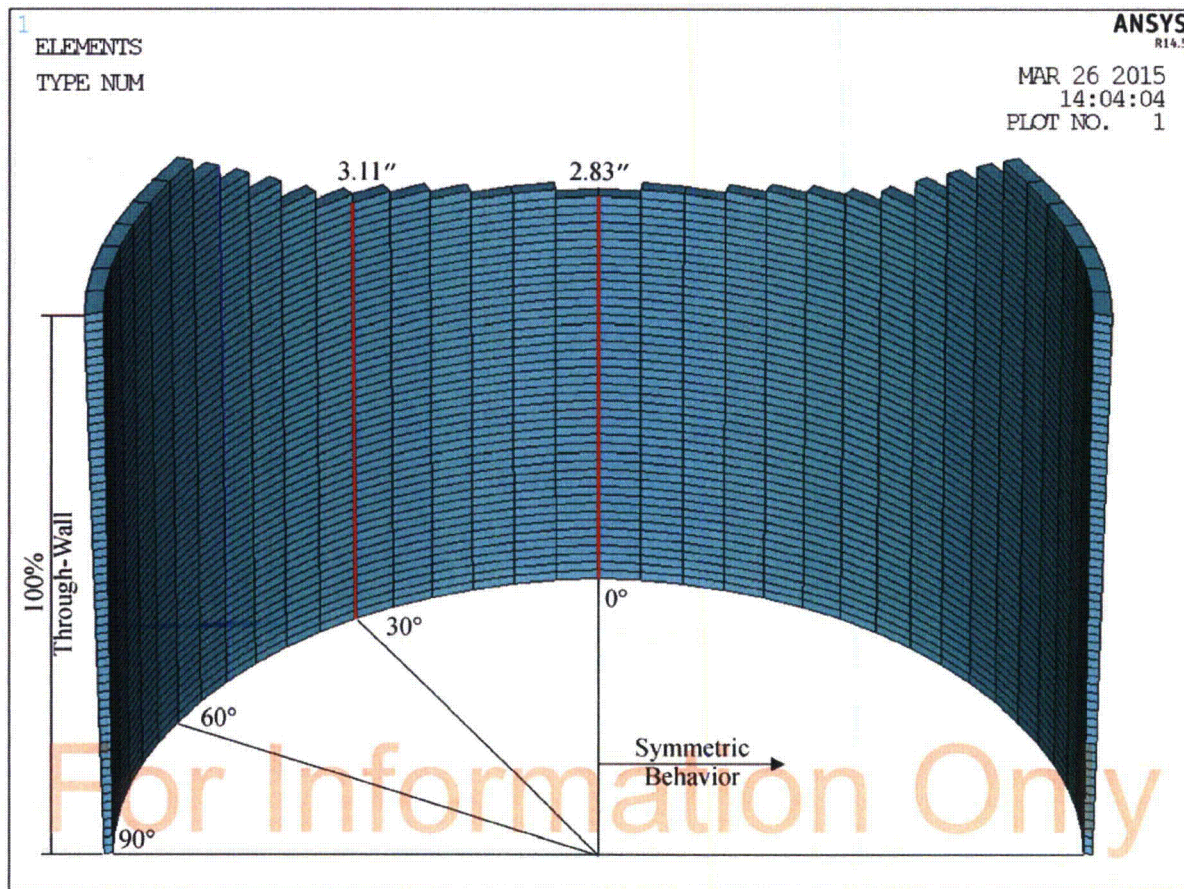


Figure 10. Extent of Partial-Arc Through-wall Circumferential Flaw Assumed for Limit
Analysis
(ASME Code, Level A Service Limits)

Note: Flaw is Located at the Nozzle-Weld Interface.

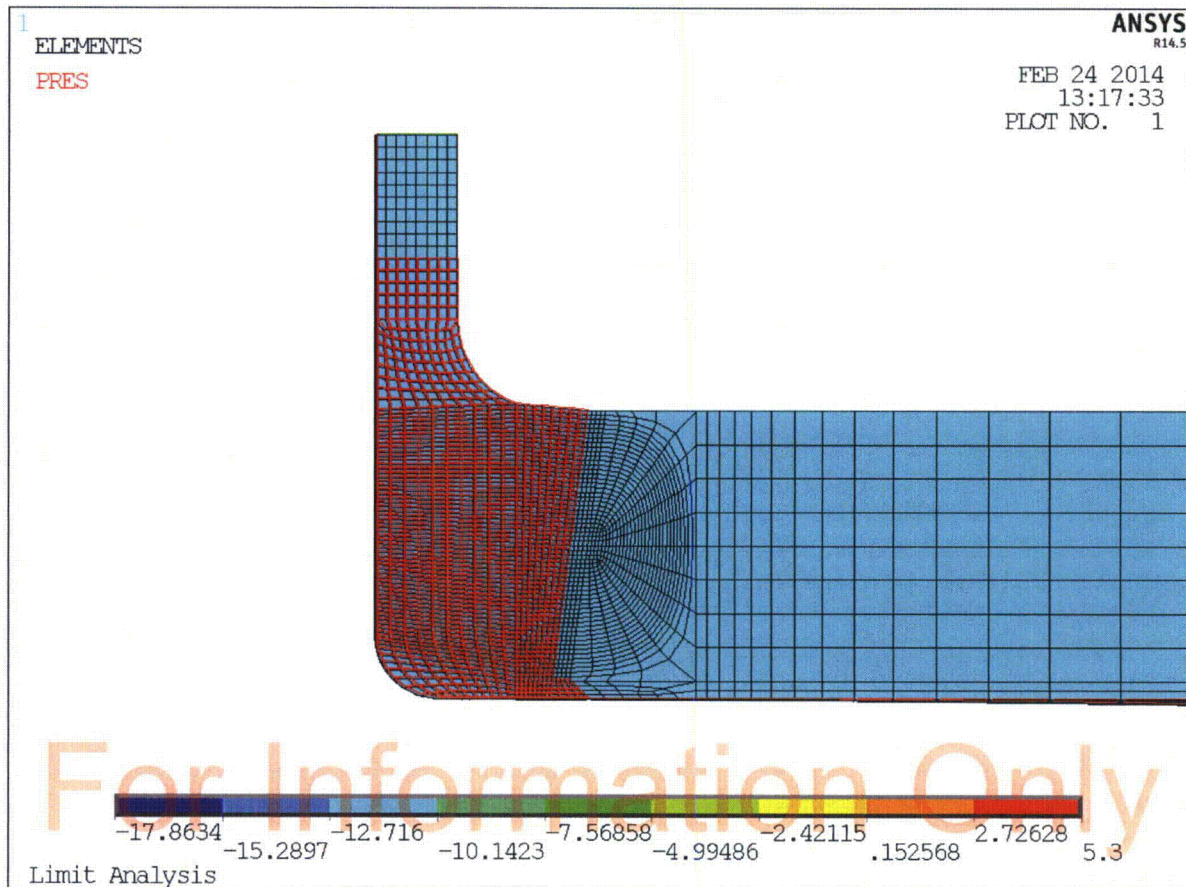


Figure 11. Extent of Through-Wall Axial Flaw Assumed for Limit Analysis
(ASME Code, Level A Service Limits)



5215 Hellyer Ave.
Suite 210
San Jose, CA 95138-1025
Phone: 408-978-8200
Fax: 408-978-8964
www.structint.com
rbax@structint.com

May 8, 2015

Report No. 1400669.404.R0

Quality Program: ☒ Nuclear ☐ Commercial

William Sims
Director, Chief Engineer
Major Projects
1448 S.R. 333
Russellville, Arkansas
72802

Subject: Additional Evaluations of the Palisades Nuclear Plant Hot Leg Drain Nozzle for Primary Water Stress Corrosion Cracking

- References:
- 1) Structural Integrity Associates Memorandum RLB-14-001, "Additional Evaluations of the Palisades Nuclear Plant Hot Leg Drain Nozzle for Primary Water Stress Corrosion Cracking," dated March 9, 2014, SI File No. 1200895.410.
 - 2) Structural Integrity Associates Calculation No. 1200895.306, Revision 1, "Hot Leg Drain Nozzle Weld Residual Stress Analysis and Circumferential Crack Stress Intensity Factor Determination."
 - 3) Structural Integrity Associates Calculation No. 1200895.307, Revision 1, "Hot Leg Drain Nozzle Crack Growth Analyses."
 - 4) Structural Integrity Associates Calculation No. 1200895.308, Revision 1, "Hot Leg Drain Nozzle Limit Load Analyses for Flawed Nozzle-to-Hot Leg Weld."
 - 5) Structural Integrity Associates Report No. 1400699.403, Revision 0, "Evaluation of the Palisades Nuclear Plant Hot Leg Drain Nozzle for Primary Water Stress Corrosion Cracking."
 - 6) Structural Integrity Associates Memorandum RAM-14-008, "Evaluation of the Palisades Nuclear Plant Hot Leg Drain Nozzle for Primary Water Stress Corrosion Cracking," dated February 25, 2014, SI File No. 1200895.408.
 - 7) Relief Request Number RR 4-18, "Proposed Alternative, Use of Alternate ASME Code Case N-770-1 Baseline Examination," PNP 2014-015, February 25, 2014.
 - 8) Palisades Document No. EC-LATER, Revision 0, "Design Input Record," SI File No. 0801136.202.

Toll-Free 877-474-7693

Chicago, IL
877-474-7693

Akron, OH
330-899-9753
Denver, CO
303-792-0077

Austin, TX
512-533-9191
San Diego, CA
858-455-6350

Charlotte, NC
704-597-5554
San Jose, CA
408-978-8200

Chattanooga, TN
423-553-1180
State College, PA
814-954-7776

Toronto, Canada
905-829-9817

Additional Evaluations of the Palisades Nuclear Plant Hot Leg Drain Nozzle for Primary Water Stress Corrosion Cracking

- 9) NMC Calculation No. EA-FC-977-01, Revision 2, "Reactor Power Uprate from Improved Thermal Power Measurement," June 15, 2006, SI File No. 1200895.218.
- 10) Email from Dave McMaster (Entergy) to Richard Bax (SI), "Subject: FW: Additional Crack Growth Evaluations," dated March 7, 2014, including attached document "*Reactor Head projected EDY at end of 1R24.doc*," SI File No. 1200895.222.
- 11) Letter from G. White (Dominion Engineering, Inc.) to W. Sims (Entergy), "Initial Flaw Assumption for Alloy 82/182 Full-Penetration Branch Pipe Connection Weld at Palisades," DEI Letter L-4199-00-02, Rev. 0, dated March 9, 2014, SI File No. 1200895.219.
- 12) ASME Boiler and Pressure Vessel Code, Section XI, *Rules for Inservice Inspection of Nuclear Power Plant Components*, 2001 Edition with Addenda through 2003.
- 13) Letter from G. White (Dominion Engineering, Inc.) to W. Sims (Entergy), "Effect of Post-Weld Heat Treatment Applied to Alloy 82/182 Full-Penetration Branch Pipe Connection Welds at Palisades," L-4199-00-01, Rev. 0, dated February 25, 2014, SI File No. 1200895.219.
- 14) Amzallag, C., Boursier, J., Pages, C., and Gimond C., "*Stress Corrosion Life Assessment of 182 and 82 Welds used in PWR Components*," Tenth International Conference on Environmental Degradation of Materials in Nuclear Power Systems, Water Reactor," © 2002 NACE International.

Dear William,

The original Memorandum, RLB-14-001 [1], has been revised and reissued as a Letter Report to incorporate new circumferential and axial crack growth evaluations that were developed due to an error in an earlier weld residual stress analysis, which generated an inaccurate residual stress field and resulted in un-conservative crack growth durations.

The original series of Structural Integrity (SI) calculations, Reference 2, 3 and 4 (in Revision 0 form) were revised and the initial results updated in Reference 5 in order to justify that there was no structural integrity/safety issues resulting from circumferential and axial-radial flaws in the Alloy 182 small bore nozzle-to-main loop piping weld that were assumed to initiate at plant startup and grow due to Primary Water Stress Corrosion Cracking (PWSCC).

The original inaccurate results, documented in Reference 6, were submitted to the Nuclear Regulatory Commission (NRC) as part of Relief Request Number RR 4-18 [7]. During a conference call with the NRC staff on March 7, 2014, the NRC staff expressed concerns about the potential for leakage from an axial flaw. The NRC staff indicated that in addition to demonstrating reasonable assurance of structural integrity, a second criterion is to demonstrate reasonable assurance of leak tightness over the operating period covered by the relief request.

Finally, the NRC staff indicated its preference that the residual stresses, assumed in the crack growth calculation, should reflect the presence of a substantial ID weld repair at the hot leg drain nozzle-to-hot leg piping weld.

In response, SI performed additional PWSCC based crack growth evaluations with increased hoop stresses, which are intended to bound the effects of any weld repairs that might be present in order to demonstrate reasonable assurance of leak tightness. The evaluations conservatively do not take credit for time to crack initiation or crack growth rate reductions due to Post Weld Heat Treatment (PWHT). The revised crack growth calculations also remove unnecessary conservatisms previously assumed with regard to operating temperature and the initial flaw depth. These additional evaluations and results have been updated in response to the original residual stress error and included as part of the revision in Reference 3.

Revised Evaluation Descriptions

The additional evaluations, documented in Reference 3, altered the following inputs to the original crack growth evaluation (Run 0 in the Table below):

Temperature

The original crack growth evaluation for the axial flaw used a hot leg temperature (T_{hot}) of 593°F, which was based on the Palisades Design Input Record No. EC-LATER [8]. The document and temperature in question is the plant design normal operating temperature, which was used for the design and safety calculations. This value does not represent the actual operating temperature as plants can operate at lower T_{hot} values.

NMC Calculation EA-FC-977-01 [9, Attachment 1, page 6] indicates that a Pre-Uprate T_{hot} was 582.7°F, and the Post-Uprate T_{hot} is 583°F. Therefore, additional crack growth evaluations will be performed using 583°F. Additional analyses were performed at 580°F to evaluate the impact of additional temperature reduction on the crack growth.

It should be noted, that per Palisades document *Reactor Head projected EDY at end of 1R24* [10] the reactor head temperature at the end of Cycle 9 (end of cycle: 2/6/1992) was 586.4°F, which is a difference of approximately $(586.4 - 582.7) = 3.7^\circ\text{F}$ between head and hot leg. During cycles 1 and 2 (12/31/1971 to 12/20/1975 and 5/9/1976 to 1/6/78) the head temperature was 569°F and 575°F, respectively. This would result in hot leg temperatures of approximately 565.3°F and 571.3°F, which are 17.7°F and 11.7°F less than was analyzed for the 583°F case. Considering these reduced temperatures during early operation, the crack growth evaluations for 580°F and 583°F will tend to be conservative as less crack growth would initially occur.

Reduced Initial Flaw Depth

The original crack growth evaluation for the axial flaw used an initial flaw depth of 0.1 inches. This initial flaw size was chosen arbitrarily as simply a small flaw. However, as documented in a letter by Dominion Engineering, Inc. [11], under the very conservative assumption of a flaw that has initiated immediately upon plant startup, an initial flaw depth of 0.025 inches may appropriately be assumed. Extensive laboratory PWSCC crack growth rate testing has demonstrated that long crack growth behavior is exhibited for flaws with depths of only 0.002 inches.

Note that for these additional axial flaw crack growth evaluations, the surface length will be held constant at 2 inches, which produced the lowest axial crack growth life of 11.3 years (to 75% through-wall) in Reference 3. Considering the geometry of the hot leg drain nozzle and its stress field, the assumed constant surface length of 2 inches is considered a conservative assumption, as the root of the hot leg drain nozzle-to-hot leg piping weld is approximately 0.5 inches wide, which leaves 1.5 inches of the flaw in the Alloy 600 nozzle body, which would have a slower PWSCC crack growth rate than the Alloy 182 weld material.

Modified Hoop Stress Profiles to Address the Possibility of a 50% Through-Wall Weld Repair

During the NRC conference call, it was indicated that an independent residual stress evaluation had included an ID weld repair. The stresses at the ID were reported to have been reduced, but the through-wall stresses were about 5 ksi larger than that generated in SI's original residual stress results submitted with the Relief Request [7].

To account for a weld repair, a second hoop stress profile was also evaluated. The new profile was simply the original profile, increased uniformly by 5 ksi (tensile) and conservatively did not attempt to take credit for the lower ID stresses. In this manner, the new hoop profile conservatively bounds the potential presence of a large weld repair on the weld ID.

Flaw Depth Allowed to Grow to 93.125% versus 75%

The original crack growth evaluation for the axial flaw halted the growth evaluation at 75% of the nominal thickness (i.e. 3 inches). For the evaluations for T_{hot} equal to 583°F, the flaw will be allowed to grow to 3.725 inches (93.125% of nominal wall) instead of stopping at 3 inches. The limit of 3.725 inches is based the extent of the hoop stress field data that was extracted in Reference 3 (see Figure 1). The originally assumed end point of a 75% through-wall flaw corresponds to the maximum flaw depth allowed by the ASME Code, Section XI [12]. However, an axial flaw that is 93.125% through-wall also meets the criterion of demonstrating leak tightness.

Crack Growth Evaluations

Thus a total of 4 crack growth evaluations were run: the two temperatures with the Original stress field, and the new flaw depth and the two temperatures with the revised stress field (original + 5 ksi) and the new flaw depth.

In addition, flaw growth out to a depth of 3.725 inches (93.125% through-wall) as well as 3 inches (75% through-wall) were reported.

The results and methodology are documented in Reference 3.

Crack Growth Results

The results of the additional crack growth evaluations are provided in the following table:

Run #	Stress Field	Initial Flaw Depth (inches)	Temperature (°F)	Time (yrs) to crack to a given depth	
				75%	93.125%
0	Original ⁽¹⁾	0.1"	593	11.3	---
1	Original ⁽¹⁾	0.025"	580	16.9	22.3
2	Original ⁽¹⁾	0.025"	583	15.6	20.7
3	Original + 5 ksi ⁽²⁾	0.025"	580	12.8	16.6
4	Original + 5 ksi ⁽²⁾	0.025"	583	11.8	15.4

Notes:

- 1) "Original" indicates the stress field generated in Reference 2, Table 11.
- 2) "Original + 5 ksi" adds 5 ksi of tensile stress to the "Original" stress field results.

As an example, the K values for the 3.725 inch crack depth cases, Runs 1 through 4, are shown in Figure 2 and their corresponding crack growth results shown Figure 3.

A direct comparison between Run 0 and Run 1 shows that the reduction of temperature and initial flaw size produces a beneficial effect on the crack growth time. Compared to the original analysis, Run 0, to Run 1, the crack growth time increases from 11.3 years to 16.9 years to reach 75% through-wall.

A direct comparison of the "Original + 5 ksi" stress field evaluation, Run 3, to Run 0 actually increased the crack growth time, but not significantly, only increasing the original 11.3 years to 12.8 years. It should be noted that the use of a generic increase of 5 ksi across the entire original stress field (i.e., full thickness) is very conservative. It should also be noted the advantage of the reduction in temperature from 593°F to 580°F on PWSCC growth rate.

For the more accurate/realistic evaluations (i.e. actual operating temperature, and growth out to 93.125%, Runs 2 and 4), the crack growth results exceeded the results for the 580°F, 75% through-wall evaluations (Runs 1 and 3). The improvement is 20.7 years vs. 16.9 years for original hoop stress field and 15.4 years vs. 12.8 years for original + 5 ksi hoop stress field. This is despite the fact that Runs 2 and 4 are evaluated at the slightly greater temperature of 583°F. It should again be noted that during the plants operation from 12/31/1971 to 1/6/1978 [10], the hot leg temperatures were approximately 17.7°F and 11.7°F less than was analyzed. Inclusion of these lower temperatures for the given time periods would further increase the crack growth time.

It is also recognized that there is still an additional 0.275 inches of base material available to grow through, before onset of leakage that was not included in the Run 2 and 4 evaluations.

Extrapolating from Figure 3, for the Original Stress Field (Run 2), it is estimated that a total crack growth time of approximately 22.5 years is required to grow the flaw to 4 inches (i.e.

through-wall). For the Original Stress Field + 5 ksi (Run 4), it is estimated that a total crack growth time of approximately 17 years is required to grow the flaw through-wall.

Conclusions

Using accurate operating conditions and a more appropriate initial flaw size and allowing the flaw to actually grow through-wall, a crack growth evaluation was performed, which indicates that the total time to grow through-wall through-wall is 22.5 years when using the hoop stress field generated in Reference 2.

Since the SI generated hoop residual stress field did not include an ID weld repair, a second evaluation was performed with the hoop stress field uniformly increased by 5 ksi (tensile). Using this conservative stress field the total time to grow through-wall is 17 years.

Finally, the resulting crack growth time is in terms of years of time during which the reactor is at operating pressure and temperature and not simply years since licensed to operate. Per Reference 10, the total Effective Full Power Years (EFPY) at the end of the next refueling outage (1R24) is expected to be 27.61. However, this result is still greater than the 22.5 years when using the original stress field (Run 2) and the 17 years for original + 5 ksi stress field.

Note that all of the analysis described above do not include the beneficial effects of reduced PWSCC crack growth rate in Alloy 82/182 weld material that have been subjected to PWHT. As documented in a second letter by Dominion Engineering, Inc. [13], on the basis of laboratory PWSCC crack growth rate testing, French research investigators have developed a disposition equation that includes a factor of 2 reduction in the crack growth rate as a function of K for Alloy 182 that has been exposed to PWHT. Using such a factor would increase crack growth time to 45 years for the original hoop stress field and 34 years for the original + 5 ksi stress field. Based on these durations, there is 17.4 EFPY margin (45 EFPY - 27.6 EFPY) for an axial flaw to leak based on the original stress field and a 6.4 EFPY margin (34 EFPY - 27.6 EFPY) for original + 5 ksi stress field.

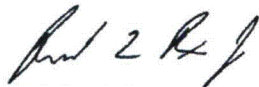
In addition, all of the analysis presented do not take into account the time to crack initiation. The results assume that an initial flaw (0.025" or 0.10") exists at plant startup. Figure 4 shows crack initiation time verses stress in Alloy 182 material. The plot shows a threshold just above 400 MPa (58 ksi). The maximum ID surface stresses for these components are in the range of 36 to 40 ksi (250 to 275 MPa) as shown in Figures 4 and 5 of Reference 5. Figure 4 shows that in the range of 250 to 275 MPa no cracks occurred. The longest duration on the figure in which no initiation occurred is in the order to 10^5 hours. For this evaluation it is conservatively assumed that initiation would not occur for at least 10^5 hours or 11.4 EFPY. Therefore, the total duration for a flaw to initiate and grow through-wall will be increased by 11.4 EFPY.

The final duration for a flaw to initiate and grow through-wall, including the effects of PWHT on Alloy 82/182 weld material, is 56 EFPY (45 EFPY + 11 EFPY), based on the original stress field, and 45 EFPY (34 EFPY + 11 EFPY) for the original + 5 ksi stress field.

Additional Evaluations of the Palisades Nuclear Plant Hot Leg Drain Nozzle for Primary Water
Stress Corrosion Cracking

In summary, the crack growth evaluations demonstrate reasonable assurance of leak tightness, in addition to reasonable assurance of structural integrity, for a period well beyond that covered by the relief request (i.e., one future cycle of operation).

Prepared by:

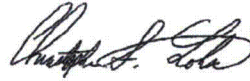


Richard Bax
Associate

5/8/2015

Date

Verified by:



Chris Lohse
Senior Consultant, P.E.

5/8/2015

Date

Approved by:



Richard Mattson
Senior Associate, P.E.

5/8/2015

Date

For Information Only

cc: Norman Eng
Christine King

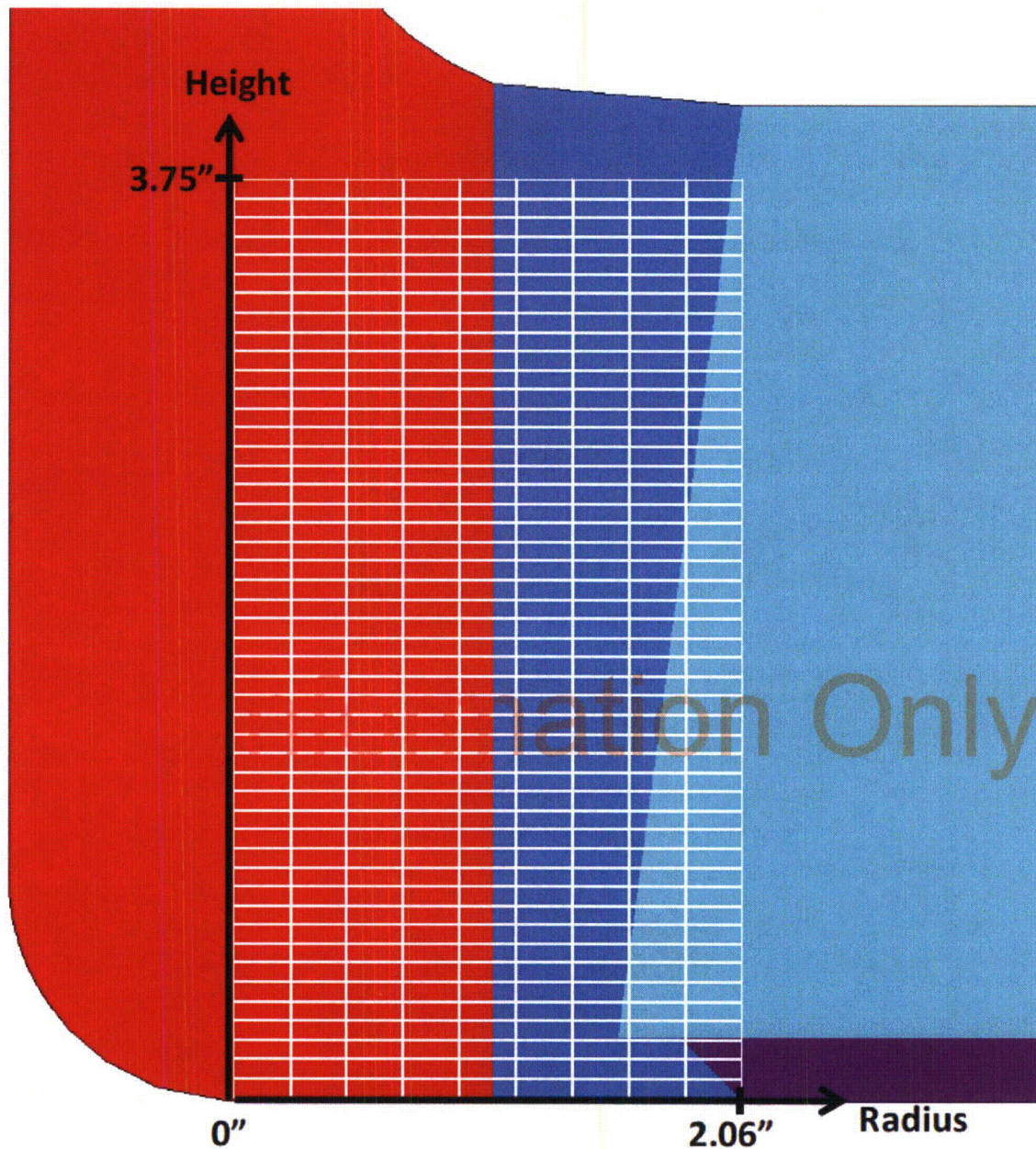


Figure 1 – Hoop Stress Extraction Grid for Axial Crack Growth Evaluation

(Figure is reproduced from Reference 2, Figure 20)

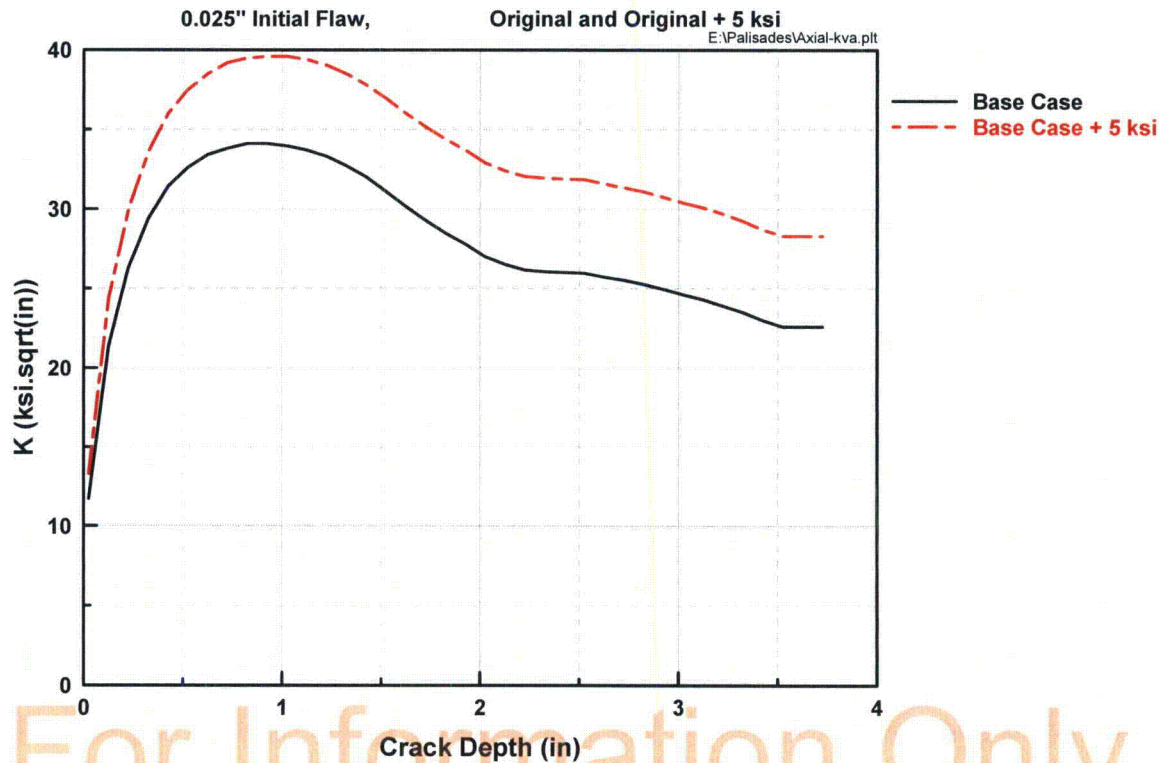


Figure 2 – *SmartCrack* Stress Intensity Factors for Axial Cracks (Runs 2 and 4)

(0.025 inch Initial Flaw, Original or Original + 5 ksi Stress Field)

Additional Evaluations of the Palisades Nuclear Plant Hot Leg Drain Nozzle for Primary Water
Stress Corrosion Cracking

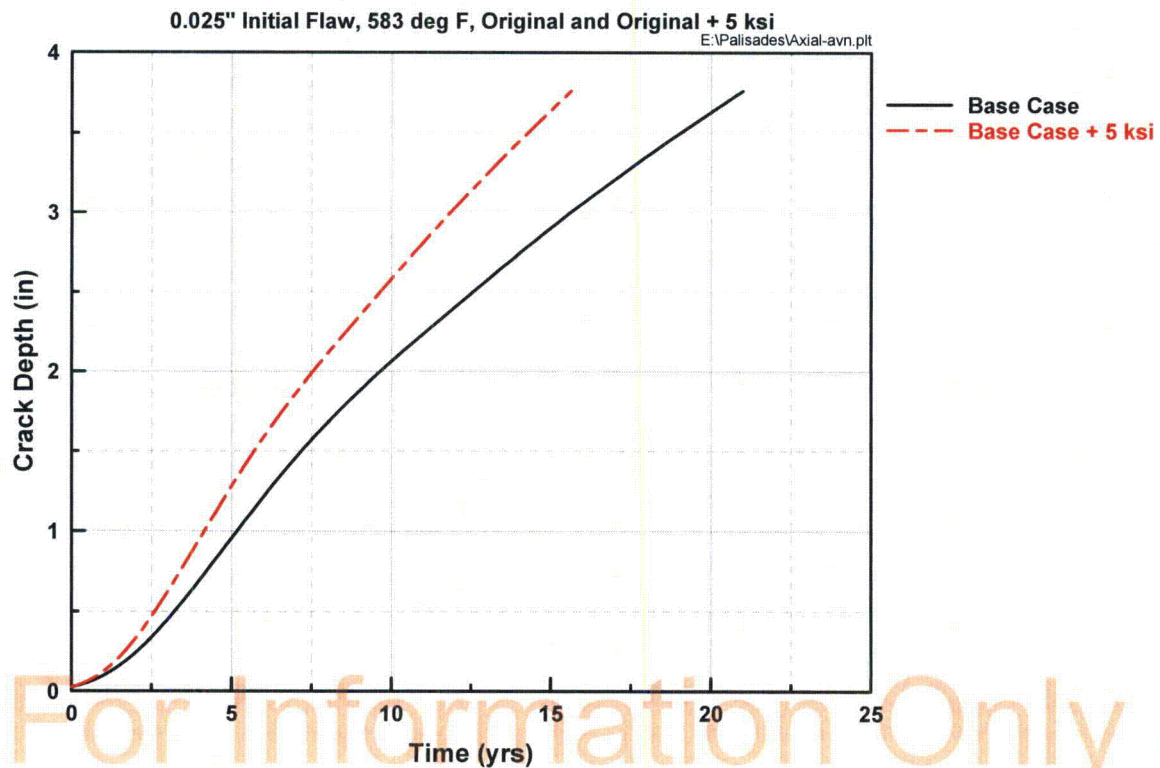


Figure 3 – Crack Depth vs. Time for the Growth of Axial Cracks (Runs 2 and 4)

(0.025 inch Initial Flaw, 583°F, Original or Original + 5 ksi Stress Field, 3.725 inch depth)

Additional Evaluations of the Palisades Nuclear Plant Hot Leg Drain Nozzle for Primary Water Stress Corrosion Cracking

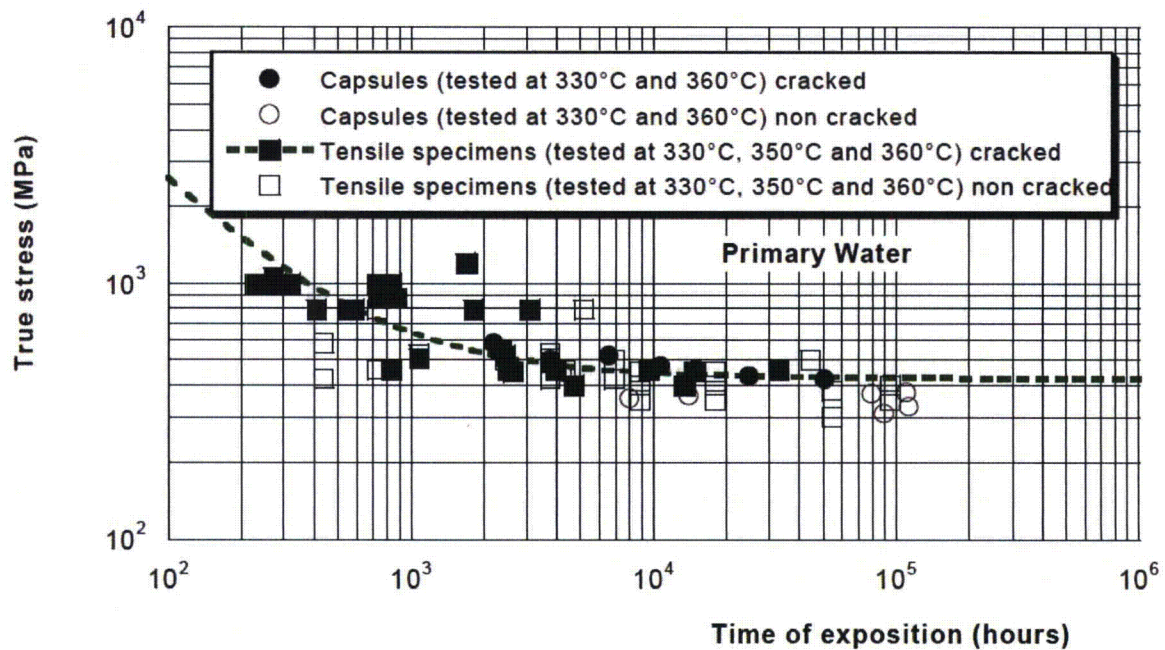


Figure 4 – Crack Initiation Time as a Function of Stress for Alloy 182 in Primary Water Environment [14, Figure 5]



Structural Integrity Associates, Inc.®

CALCULATION PACKAGE

File No.: 1200895.306

Project No.: 1400148

Quality Program: ☒ Nuclear ☐ Commercial

PROJECT NAME:

Evaluation of Hot Leg Drain Nozzle

CONTRACT NO.:

10404220

CLIENT:

Entergy Nuclear

PLANT:

Palisades Nuclear Plant

CALCULATION TITLE:

Hot Leg Drain Nozzle Weld Residual Stress Analysis and Circumferential Crack Stress Intensity Factor Determination


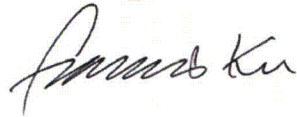
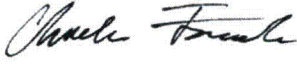
Document Revision	Affected Pages	Revision Description	Project Manager Approval Signature & Date	Preparer(s) & Checker(s) Signatures & Date
0	1 – 45 A-1 – A-4	Initial Issue	Richard Bax RLB 03/06/14	Francis Ku FHK 03/06/14 Charles Fourcade CJF 03/06/14
1	5-12, 14, 16, 19-22, 24, 25 36 – 38 40 – 44 A-3, A-4	Corrected pressure error in Hydrostatic Test and Normal Operating Cycle steps.	 Gole Mukhim GSM 5/8/15	 Francis Ku FHK 5/8/15  Charles Fourcade CJF 5/8/15

Table of Contents

1.0	OBJECTIVE	5
2.0	TECHNICAL APPROACH	5
2.1	Material Properties.....	5
2.2	Finite Element Model for Weld Residual Stress Analysis	6
2.3	Finite Element Models with Circumferential Flaws.....	6
2.4	Welding Simulation	6
2.5	Heat Inputs	7
2.6	Creep Properties.....	7
2.7	Mechanical Load Boundary Conditions	8
3.0	ASSUMPTIONS.....	8
4.0	WELD RESIDUAL STRESS ANALYSIS	9
4.1	Hot Leg Cladding	10
4.2	Boss Main Weld	10
4.3	ID Patch Weld.....	10
4.4	Post Weld Heat Treatment.....	10
4.5	Hydrostatic Test.....	11
4.6	Five Normal Operating Cycles (NOC)	11
5.0	RESULTS OF WELD RESIDUAL STRESS ANALYSIS.....	12
5.1	Welding Temperature Contours	12
5.2	PWHT Temperature Results.....	12
5.3	Residual Stress Results	12
6.0	K CALCULATION FOR CIRCUMFERENTIAL CRACKS.....	13
6.1	Crack Face Pressure Application.....	13
6.2	Circumferential Crack Stress Intensity Factor Results.....	14
7.0	STRESS EXTRACTION FOR AXIAL CRACKS	14
7.1	Hoop Stress Extraction for Axial Crack Growth Evaluation.....	14
8.0	CONCLUSIONS	15
9.0	REFERENCES	16
	APPENDIX A COMPUTER FILES LISTING.....	A-1

List of Tables

Table 1: Elastic Properties for SA-516 Grade 70 (≤ 4 " Thick)	17
Table 2: Elastic Properties for ER308L	17
Table 3: Elastic Properties for Alloy 600	18
Table 4: Elastic Properties for Alloy 82/182	18
Table 5: Stress-Strain Data for SA-516 Grade 70 (≤ 4 " Thick)	19
Table 6 Stress-Strain Data for ER308L	20
Table 7: Stress-Strain Data for Alloy 600	21
Table 8: Stress-Strain Data for Alloy 182	22
Table 9: Creep Properties	23
Table 10: Circumferential Crack "K vs. a" Table	24
Table 11: Hoop Stress Table at 0° Azimuth for Axial Crack Growth Evaluation	25

For Information Only

List of Figures

Figure 1: Finite Element Model for Residual Stress Analysis	26
Figure 2: Finite Element Model for the 0.13” Deep Circumferential Crack	27
Figure 3: Applied Mechanical Boundary Conditions	28
Figure 4: Weld Nugget Definitions for the Boss Main Weld	29
Figure 5: Weld Nugget Definitions for the ID Patch Weld	30
Figure 6: Applied Hydrostatic and Corresponding End Cap Pressure Loads	31
Figure 7: Predicted Fusion Boundary Plot for Cladding	32
Figure 8: Predicted Fusion Boundary Plot for Boss Main Weld	33
Figure 9: Predicted Fusion Boundary Plot for ID Patch Weld	34
Figure 10: Temperature Curve for PWHT.....	35
Figure 11: Predicted von Mises Residual Stress after ID Patch Weld at 70°F	36
Figure 12: Predicted von Mises Residual Stress after PWHT at 70°F	37
Figure 13: Residual Stress Comparison for Before and After PWHT.....	38
Figure 14: Measured Through-Wall Residual Stresses for PWHT	39
Figure 15: Predicted von Mises Residual Stress after Hydrostatic Test at 70°F	40
Figure 16: Predicted Radial Residual Stress + Operating Conditions (5 th NOC Cycle)	41
Figure 17: Predicted Hoop Residual Stresses + Operating Conditions (5 th NOC Cycle).....	42
Figure 18: Transferred Radial Residual + NOC + Pressure Stresses (3.95” Crack Shown) ..	43
Figure 19: FEA Calculated Circumferential Crack “K vs. a” at Four Azimuth Locations	44
Figure 20: Hoop Stress Extraction Grid for Axial Crack Growth Evaluation.....	45

1.0 OBJECTIVE

The objective of this calculation package is to document the revised weld residual stress analysis and the resulting circumferential crack stress intensity factor determination for the hot leg drain nozzle at the Palisades Nuclear Plant (Palisades).

The revised weld residual stress analysis is based on the latest methodology and process developed by Structural Integrity Associates (SI). The stress intensity factor determination is performed using finite element analysis (FEA) for a full circumferential crack in the nozzle-to-hot leg dissimilar metal weld.

Revision 1 corrects an error in the pressure application for the hydrostatic test and normal operating cycle load steps.

2.0 TECHNICAL APPROACH

The finite element model is obtained from a previous project for Palisades [1] and the weld residual stress analysis repeats the steps in the previous weld residual analysis [2], but uses the latest weld residual stress analysis methodology and process developed by SI.

The circumferential flaws are modeled in this calculation and evaluated by finite element analyses. Hoop stress results in the weld region, corresponding to the hot leg, from the weld residual stress analysis are extracted to evaluate axial flaws (i.e. flaws aligned with the hot leg axis), which will be performed in a separate calculation package.

The finite element model includes all components in the post-nozzle installation stage because new elements cannot be added during an ANSYS FEA. Since all the weld elements need to be included in the initial model, the element "birth and death" technique in ANSYS is used to initially deactivate the weld elements, with elements corresponding to the active weld segment reactivated at the melting temperature, thus simulating the weld metal deposition.

2.1 Material Properties

The revised weld residual stress analysis performed in this calculation uses the material properties specifically developed in a separate calculation package for weld residual stress analyses [3]. Per the material designation used in the previous project [1], the following materials are used:

- SA-516 Grade 70: Hot leg base metal
- ER308L: Hot leg cladding (typical weld metal for Type 304)
- Alloy 82/182: Boss main weld and ID patch weld
- Alloy 600 (SB-166): Drain nozzle

The material properties for the above materials are tabulated in Tables 1 through 8.

2.2 Finite Element Model for Weld Residual Stress Analysis

The finite element model for the analyses was developed in a previous project for Palisades [1], which was created using a legacy version of the ANSYS finite element analysis software package [4]. The finite element model is recreated using a newer version of ANSYS [5] for the analyses in this calculation to take advantage of the solver and speed enhancements in the newer software release.

The base finite element model for the weld residual stress analysis is meshed with 8-node solid elements (SOLID185) in ANSYS. This finite element model is shown in Figure 1.

2.3 Finite Element Models with Circumferential Flaws

The intent of the residual stress analysis is to evaluate the fracture mechanics characteristics of postulated flaws through the nozzle boss weld. The stress intensity factors for a full circumferential flaw in the nozzle boss weld are determined by finite element analysis using deterministic linear elastic fracture mechanics (LEFM) principles. As a result, seven fracture mechanics finite element models are derived to include “collapsed” crack meshing that represent full (360°) circumferential flaws surrounding the nozzle at various depths within the boss weld.

The circumferential cracks align with the interface between the boss weld and the nozzle. The modeled crack depths are: 0.13”, 0.57”, 1.21, 1.85”, 2.49”, 3.13”, and 3.95”.

The modeling of the flaws, or cracks, involves splitting the crack plane and then inserting “collapsed” mesh around the crack tips followed by concentrated mesh refinements that surround the “collapsed” mesh, and are referred to as “crack tip elements”. This step is implemented on a source finite element model without the cracks, which is referred to as the “base model”, and then the crack tip elements are inserted by an in-house developed ANSYS macro (see Appendix A for file listing).

For the fracture mechanics models, 20-node quadratic solid elements (SOLID95) are used in the crack tip region, while 8-node solid elements (SOLID45) are used everywhere else in the model. The mid-side nodes for the SOLID95 elements around the crack tips are shifted to the “quarter point” locations to properly capture the singularities at the crack tips, consistent with ANSYS recommendations. The finite element model for the 0.13” deep crack, with the crack tip mesh, is shown in Figure 2 as an example; the crack tip mesh for the other crack depths follows the same pattern.

The quarter point mid-side nodes combined with the extra layers of concentrated elements around the crack tips, as shown in Figure 2, provide sufficient mesh refinement to determine the stress intensity factors for the fracture mechanics analyses.

2.4 Welding Simulation

The FEA for predicting the weld residual stresses is performed as a continuous analysis so that the load history from the cladding is carried over to the boss main weld and then the ID patch weld. Specifically,

the residual stresses and strains at the end of one weld pass are used as initial conditions for the next weld pass.

The procedures for this complex multi-step simulation are encoded in ANSYS Parametric Design Language (APDL) macros which utilize elastic-plastic material behavior and elements with large deformation capability to predict the residual stresses due to the various welding processes.

2.5 Heat Inputs

The deposition of the weld metal is simulated by imposing a heat generation function on the elements representing the active weld, which is applied as a volumetric body heat generation rate. The amount of equivalent heat input energy, Q (in terms of kJ/inch), is determined from the welding parameters.

Since the welding parameters for the welds are not available, a typical heat input of 28 kJ/in, with an overall heat efficiency of 0.8, is assumed for all of the welds. The heat efficiency represents a “composite” value reflecting the concepts of arc efficiency, melting efficiency, etc., and is an optimum value to produce reasonable heat penetration in the analysis.

The APDL macros automatically calculate the appropriate cooling time intervals for the thermal pass to ensure that sufficient heat penetration is achieved, the required interpass temperature between weld passes is met, and a reasonable overall temperature distribution within the finite element model is achieved. The resulting temperature time history is then imported into the stress pass in order to calculate the residual stresses due to the thermal cycling of the weld elements using nonlinear, elastic-plastic load/unload stress reversal relations.

The following summarizes the welding parameters used in the analysis:

- Interpass temperature = 350°F
- Melting temperature = 2500°F
- Ambient temperature = 70°F
- Heat input for all welds = 28 kJ/in
- Heat efficiency for all welds = 0.8
- Inside/Outside heat transfer coefficient = 5 Btu/hr-ft²-°F
- Inside/Outside temperature = 70°F

2.6 Creep Properties

Strain relaxation due to creep at high temperature is considered in the post weld heat treatment (PWHT) step. In general, creep becomes significant at temperatures above 800°F; thus, creep behavior under 800°F will not be considered in this analysis.

There are two main categories of creep: primary and secondary. The primary creep addresses the creep characteristics for a short duration at the early stages of the creep regime, while the secondary creep

accounts for the creep behavior for a long duration – usually more than 10,000 hours. Based on this definition, the PWHT falls within the primary creep characteristics. However, primary creep rates for materials are difficult to obtain, so the conservative secondary creep rates are used since primary creep rate is typically an order of magnitude higher than that for secondary creep.

In general, the primary creep rate for the materials is governed by the equation:

$$\frac{d\varepsilon}{dt} = A\sigma^n$$

The creep data for the SA-516 Grade 70 hot leg material is based on carbon steel material [6]. The creep data for the Alloy 82/182 and ER308L weld metals are not available, so the creep properties for their base metals are used instead. The creep data for Type 304 (for ER308L) is provided in the same reference as the carbon steel [6], while the creep data for the Alloy 600 (for Alloy 82/182) is provided in a separate publication [7]. All the creep strengths, σ , are provided at two creep rates [6, 7] for each temperature point.

When creep strength is provided at two creep rates at the same temperature point, as listed in Table 9, then A and n can be calculated as follows, where subscripts 1 and 2 refer to the creep data sets 1 and 2:

$$\begin{aligned} \frac{d\varepsilon}{dt} &= \dot{\varepsilon} = A\sigma^n \\ \dot{\varepsilon}_1 &= A\sigma_1^n; \quad \dot{\varepsilon}_2 = A\sigma_2^n \\ \frac{\dot{\varepsilon}_1}{\dot{\varepsilon}_2} &= \left(\frac{\sigma_1}{\sigma_2}\right)^n \\ \ln\left(\frac{\dot{\varepsilon}_1}{\dot{\varepsilon}_2}\right) &= n \ln\left(\frac{\sigma_1}{\sigma_2}\right) \end{aligned} \quad \begin{aligned} n &= \frac{\ln\left(\frac{\dot{\varepsilon}_1}{\dot{\varepsilon}_2}\right)}{\ln\left(\frac{\sigma_1}{\sigma_2}\right)} \\ A &= \frac{\dot{\varepsilon}_1}{\sigma_1^n} \end{aligned}$$

2.7 Mechanical Load Boundary Conditions

For the weld residual stress and all of the LEFM analyses, the mechanical load boundary conditions for the stress analysis are symmetric boundary conditions on the symmetry planes of the model, and axial displacement couplings on the ends of the drain nozzle and hot leg piping, as shown in Figure 3.

3.0 ASSUMPTIONS

The following assumptions are used in the analyses:

- The hot leg cladding material is assumed to be ER308L, which is a common weld metal for Type 304 stainless steel cladding.

- The modeled circumferential flaws are assumed to align with the boss weld and nozzle interface, which represents a potential crack path of the susceptible material.
- The welding interpass temperature is assumed to be 350°F, which is a typical parameter for residual stress analysis.
- The metal melting temperature is assumed to be 2500°F, which is the temperature point where the strength of the material is set to near zero [3].
- The analysis is performed with an ambient temperature of 70°F.
- The exposed surface of the model is subject to a typical ambient air cooling convection film coefficient of 5 Btu/hr-ft²-°F at a bulk temperature of 70°F. The exposed surface is defined as the external surface of the model excluding the symmetry planes and geometric ends.
- The focus of this analysis is the residual stresses in the drain nozzle boss weld region, while the detailed interaction between the clad buildup and the hot leg base metal is secondary. Therefore, the clad is assumed to be fully deposited in a one-layer single pass process.
- The boss main weld is represented by an 80-bead process, as shown in Figure 4, with each bead represented by a one pass “bead ring” nugget. This approach is a common and acceptable industry practice when information regarding the bead start/stop position and sequencing are unknown.
- Similarly, the ID patch weld is represented by a 7-bead process, as shown in Figure 5, with each bead represented by a one pass “bead ring” nugget.
- For modeling simplicity, the penetration hole is present during the deposition of the clad. This is acceptable since any localized stress that would have developed without the hole is relieved when the material is removed from the pipe.
- For convenience, the modeled ID patch weld shares the same geometry as the backing ring for the main weld.

4.0 WELD RESIDUAL STRESS ANALYSIS

The weld residual stress analysis consists of a thermal analysis to determine the temperature distribution followed by a stress analysis to determine the resulting stresses. The analytical sequence described below is used in the finite element analysis, followed by detailed discussions of the steps:

1. Deposit clad on hot leg pipe inside (ID) surface.
2. Install drain nozzle, backing ring, and deposit boss main weld.
3. Remove backing ring and deposit ID patch weld.
4. Post weld heat treatment.
5. Subject the configuration to hydrostatic test.
6. Impose 5 cycles of “shake down” with normal operating temperature and pressure.

4.1 Hot Leg Cladding

The clad material is typically welded onto the inside surface of the hot leg pipe, and the nominal thickness of the clad is thicker than the typical thickness for a single weld layer used in the process. However, the focus of this analysis is on the as-welded residual stresses, while the detailed interaction between the clad buildup and the base material during the many actual weld passes is not of interest. Therefore, the clad is assumed to be fully deposited in a single pass.

At this step, only the hot leg pipe base metal elements and clad material elements are active; all other components are deactivated. At the end of the cladding application, the entire model is cooled to 70°F before the application of the boss main weld.

4.2 Boss Main Weld

The main weld connects the drain nozzle boss to the hot leg piping. As shown in Figure 4, the weld is composed of 80 nuggets deposited in 30 weld layers. In the absence of detailed weld fabrication information, a weld sequence is assumed based on standard welding practice at the time of fabrication. In particular, for every layer, the first nugget is deposited on the hot leg side, the second nugget on the nozzle side, and the remaining nuggets (if any) are added in the radial direction from hot leg to nozzle.

At this step, the drain nozzle elements and backing ring elements are reactivated, and the boss main weld nuggets are reactivated sequentially to simulate the welding process. At the end of the boss main weld, the entire model is cooled to 70°F before the application of the ID patch weld.

4.3 ID Patch Weld

The final weld step is to add the ID patch weld, which replaces the backing ring. As seen in Figure 5, the ID patch weld is composed of 7 nuggets deposited in 2 layers.

At this step, the backing ring is first deactivated to allow the residual stresses to redistribute, and the ID patch weld nuggets are reactivated sequentially to simulate the welding process. At the end of the ID patch weld, the entire model is cooled to 70°F before the application of the PWHT.

4.4 Post Weld Heat Treatment

An important reason for performing PWHT is to relieve the residual stresses from welding. PWHT is assumed to be performed as per the following procedure outlined in Article 5, paragraph 1-731.3.1-d of USA Standard B31.7 [8]:

1. Heat welded piping component to 1125°F at a heating rate of 200°F per hour.
2. Hold at temperature for approximately 4 hours (1hr/in of weld thickness).
3. Allow to cool to 600°F at a cooling rate of 200°F per hour.
4. Air-cool from 600°F to ambient.

5. A steady state load step is imposed at the end of the PWHT process.

During the PWHT, creep behavior is activated for time steps with the maximum temperature above 800°F. At the end of the PWHT, the entire model is cooled to 70°F before the application of the hydrostatic test.

4.5 Hydrostatic Test

A hydrostatic test pressure of 3.125 ksi [9, page 9] is applied after the welding. The pressure is applied on the ID surfaces of hot leg pipe and nozzle. End-cap traction loads, $P_{\text{end-cap-nozzle}}$ and $P_{\text{end-cap-hl}}$, are applied at the free ends of the drain line nozzle and hot leg piping, respectively. These are calculated based on the following expressions:

$$P_{\text{end-cap-nozzle}} = \frac{P * r_{\text{inside}}^2}{r_{\text{outside}}^2 - r_{\text{inside}}^2}$$

where,

P = Hydrostatic test pressure (ksi)
 $P_{\text{end-cap-nozzle}}$ = End cap pressure on drain line nozzle end (ksi)
 r_{inside} = Inside radius of drain line nozzle (in)
 r_{outside} = Outside radius of drain line nozzle (in)

and,

$$P_{\text{end-cap-hl}} = \frac{P * r_{\text{inside_hl}}^2}{r_{\text{outside_hl}}^2 - r_{\text{inside_hl}}^2}$$

where,

P = Hydrostatic test pressure (ksi)
 $P_{\text{end-cap-hl}}$ = End cap pressure on hot leg pipe end (ksi)
 $r_{\text{inside_hl}}$ = Inside radius of hot leg pipe (in)
 $r_{\text{outside_hl}}$ = Outside radius of hot leg pipe (in)

The applied pressure loads on the model are shown in Figure 6.

4.6 Five Normal Operating Cycles (NOC)

After the hydrostatic test, the assembled configuration is put into service and subjected to 5 cycles of shake down to stabilize the as-welded residual stresses. This step involves ramping the model from zero-load to steady-state conditions at normal operating temperature and pressure simultaneously then back to steady-state at 70°F and no pressure five times.

The applied operating pressure is 2.122 ksi and temperature is 593°F [10]. The temperature is assumed to be uniform throughout the components and operating pressure is applied as an internal pressure on the ID surface, with corresponding end cap pressures calculated using the equations in the previous section. The term “P” is replaced by the operating pressure in the expressions.

5.0 RESULTS OF WELD RESIDUAL STRESS ANALYSIS

The ANSYS input files and computer output files for the analyses are listed in Appendix A.

5.1 Welding Temperature Contours

The maximum temperature prediction contours for each weld are created using a macro **MapTemp.mac**. This type of contour plot is also called a “fusion boundary” plot because it provides an overview of the maximum temperature on each node throughout the thermal transient for each welding process. The plots are useful in visualizing the melting of weld metal and the extent of heat penetration.

The predicted fusion boundary contours for the cladding, main weld, and ID patch weld are shown in Figures 7, 8, and 9, respectively. The purple color in the plots represents elements at melting temperature; the plots show complete melting of the weld metal for each weld and slight melting of the base metal along the weld interface.

5.2 PWHT Temperature Results

Figure 10 plots the inside surface temperature curve for the PWHT process. It shows the linear 200°F/hour heating rate, four hours (240 minutes) hold time at 1125°F, 200°F/hour cooling rate at temperature above 600°F, and the air cooling to room temperature of 70°F.

5.3 Residual Stress Results

Figure 11 plots the von Mises residual stresses after welding is complete, but before PWHT. It shows extensive residual stresses of greater than 66 ksi in the weld material. However, as shown in Figure 12, after the PWHT the residual stresses in the weld have relaxed significantly, to below 41 ksi, but the residual stresses in the cladding remain essentially unchanged.

To further investigate the effects of the PWHT, before and after PWHT residual stresses are extracted along the two through-wall paths shown in Figures 11 and 12. The through-wall residual stresses are compared in Figure 13, and it shows that there is little to no stress reduction in the clad material, while there is significant stress reduction in the pipe base metal.

The PWHT results from the FEA trend comparably well with the data in EPRI report TR-105697 [12], which contains a comparable through-wall clad residual stress distribution based on experimental measurements, as shown in Figure 14. The experimental measurements were for a low alloy steel vessel with a Type 304 stainless steel clad. The data shows tensile hoop stress through the clad thickness and the base metal near the clad interface, but the hoop stress drops rapidly to compressive values at farther distances from the clad.

Figure 15 depicts the predicted von Mises residual stresses after the hydrostatic test. It shows a reduction in maximum stress when compared to the post-PWHT step: 62.24 ksi (Figure 15) versus 73.75 ksi (Figure 12), while the overall stress distributions between the two stages remain fairly similar.

Figures 16 and 17 depict the combined weld residual plus operating radial and hoop stresses at the fifth stabilization NOC cycle, respectively. The stress results at this step are used in the fracture mechanics evaluations.

6.0 K CALCULATION FOR CIRCUMFERENTIAL CRACKS

The stress intensity factors (K_s) for the circumferential cracks are calculated using the KCALC feature in ANSYS which is based on the LEFM principle. For the LEFM evaluation, only the elastic properties in Tables 1 through 4 are used in the FEA, the stress-strain curves and creep properties in Tables 5 through 9 are not used.

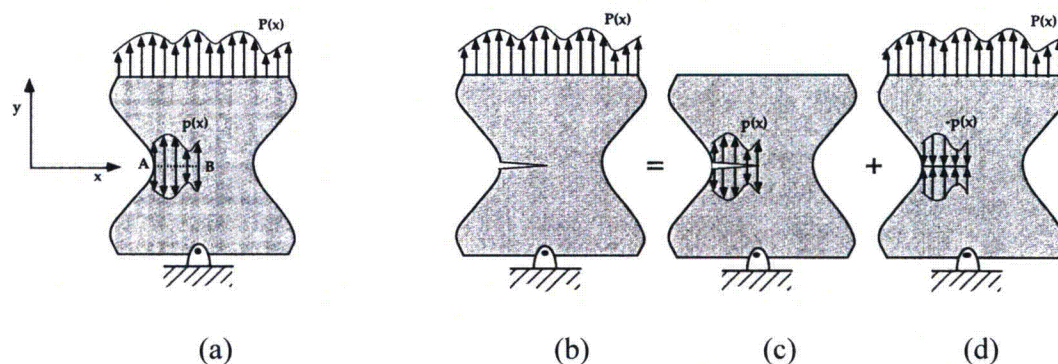
6.1 Crack Face Pressure Application

In order to determine the K_s for the circumferential cracks due to residual stresses, the stresses on the boss weld-to-nozzle interface, at the fifth operating condition (at time = 3046 minutes), are extracted from the residual stress analysis and reapplied on the crack face as surface pressure loading.

Representative transferred residual stresses onto the crack face for the deepest circumferential crack of 3.95" are shown in Figure 18.

This approach is based on the load superposition principle [11], which is utilized to transfer the stresses from the weld residual stress finite element model onto the fracture mechanics finite element model that contains crack tip elements. The superposition technique is based on the principle that, in the linear elastic regime, stress intensity factors of the same mode, which are due to different loads, are additive (similar to stress components in the same direction).

The superposition method can be summarized with the following sketches [11, page 66]:



A load $p(x)$ on an uncracked body, Sketch (a), produces a normal stress distribution $p(x)$ on Plane A-B. The superposition principle is illustrated by Sketches (b), (c), and (d) of the same body with a crack at Plane A-B. The stress intensity factors resulting from these loading cases are such that:

$$K_I(b) = K_I(c) + K_I(d)$$

Thus, $K_I(d) = 0$ because the crack is closed, and:

$$K_I(b) = K_I(c)$$

This means that the stress intensity factor obtained from subjecting the cracked body to a nominal load $p(x)$ is equal to the stress intensity factor resulting from loading the crack faces with the same stress distribution $p(x)$ at the same crack location from the uncracked body.

6.2 Circumferential Crack Stress Intensity Factor Results

The radial stresses on the weld/nozzle interface, as shown at the top of Figure 16, are transferred to the circumferential cracks as crack face pressure per the superposition principle described above.

Figure 18 depicts, as an example, the transferred radial stresses as crack face pressure for the 3.95" crack depth. During the crack face pressure transfer, the operating pressure of 2122 psi [10] is added to the crack face pressure to account for the internal pressure acting on the crack face due to cracking.

Each crack model is analyzed as a steady state stress pass at the operating and reference temperature of 593°F [10] in order to use the material properties at the operating temperature, but without inducing additional thermal stresses.

At the completion of each analysis, the ANSYS KCALC post-processing is performed to extract the K_s at each crack tip node around the nozzle. The K results are summarized in Table 10 for various crack depths "a". The "K vs. a" trend at the 0°, 30°, 60°, and 90° azimuths are then plotted in Figure 19. The results are also included in the Excel spreadsheet listed in Appendix A.

7.0 STRESS EXTRACTION FOR AXIAL CRACKS

The axial cracks in the weld region will be evaluated in a separate calculation, designated as SI Calculation No. 1200895.307. That calculation will use the hoop stresses (corresponding to the hot leg) on the model symmetry plane at the 0° azimuth location, which represents the cross section with the most tensile residual stresses, as shown in Figure 17.

7.1 Hoop Stress Extraction for Axial Crack Growth Evaluation

The stress extraction location for the axial crack is defined as a rectangular 2.06"×3.75" grid located on the axial cut plane of the hot leg (i.e., at the 0° azimuth), as shown in Figure 20. The hoop stresses at the fifth NOC cycle (with operating loads) are extracted, which are output in terms of Radius, Height, and Stress.

The extracted hoop stresses are tabulated in Table 11 for use in the separate axial crack growth evaluation. The results are also included in the Excel spreadsheet listed in Appendix A.

8.0 CONCLUSIONS

Finite element residual stress and circumferential flaw analyses have been performed on the hot leg drain nozzle boss weld at Palisades:

- The stress intensity factors for circumferential flaws along the boss/nozzle interface have been determined using finite element analysis at normal operating conditions combined with residual stresses; the stress intensity factor results are presented in Table 10 as a function of flaw depth and azimuth location.
- Hoop stresses at normal operating conditions combined with residual stresses have been extracted on the hot leg axial cut plane and tabulated in Table 11. The hoop stress results will be used in a separate calculation to determine crack growth for axial cracks in that plane.

For Information Only

9.0 REFERENCES

1. SI Calculation No. 0801136.311, Rev. 1, "Hot Leg Drain Nozzle Finite Element Model for Welding Residual Stress Estimation."
2. SI Calculation No. 0801136.312, Rev. 1, "Hot Leg Drain Nozzle Residual Stress Analysis."
3. SI Calculation No. 0800777.307, Rev. 5, "Material Properties for Residual Stress Analyses, Including MISO Properties Up To Material Flow Stress."
4. ANSYS, Release 8.1 (w/ Service Pack 1), ANSYS, Inc., June 2004.
5. ANSYS Mechanical APDL and PrepPost, Release 14.5 (w/ Service Pack 1), ANSYS, Inc., September 2012.
6. "Steels for Elevated Temperature Service," United States Steel Co., 1949.
7. Publication SMC-027, "Inconel Alloy 600," Special Metals Corp., 2004, SI File 0800777.211.
8. USA Standard B31.7, Nuclear Power Piping, 1968.
9. Combustion Engineering Specification No. 0070P-006, Rev. 2, "Engineering Specification for Primary Coolant Pipe and Fittings," SI File No. 0801136.206.
10. Palisades Document No. EC-LATER, Revision 0, "Design Input Record," SI File No. 0801136.202.
11. Anderson, T. L., "Fracture Mechanics Fundamentals and Applications", Second Edition, CRC Press, 1995.
12. EPRI Report No. TR-105697, "BWR Reactor Pressure Vessel Shell Weld Inspection Recommendations (BWRVIP-05)," September 1995.

Table 1: Elastic Properties for SA-516 Grade 70 ($\leq 4''$ Thick)

Temperature (°F)	Elastic Modulus ($\times 10^3$ ksi)	Mean Thermal Expansion ($\times 10^{-6}$ in/in/°F)	Thermal Conductivity (Btu/min-in-°F)	Specific Heat (Btu/lb-°F)
70	29.5	6.4	0.0488	0.103
500	27.3	7.3	0.0410	0.128
700	25.5	7.6	0.0369	0.138
1100	18.0	8.2	0.0290	0.171
1500	5.0	8.6	0.0218	0.198
2500	0.1	9.5	0.0014	0.204
2500.1	N/A	0.0	N/A	N/A

Density (ρ) = 0.283 lb/in³, assumed temperature independent.

Poisson's Ratio (ν) = 0.3, assumed temperature independent.

Table 2: Elastic Properties for ER308L

Temperature (°F)	Elastic Modulus ($\times 10^3$ ksi)	Mean Thermal Expansion ($\times 10^{-6}$ in/in/°F)	Thermal Conductivity (Btu/min-in-°F)	Specific Heat (Btu/lb-°F)
70	28.3	8.5	0.0119	0.116
500	25.8	9.7	0.0151	0.131
700	24.8	10.0	0.0164	0.135
1100	22.1	10.5	0.0189	0.140
1500	18.1	10.8	0.0212	0.145
2500	0.1	11.5	0.0292	0.159
2500.1	N/A	0.0	N/A	N/A

Density (ρ) = 0.283 lb/in³, assumed temperature independent.

Poisson's Ratio (ν) = 0.3, assumed temperature independent.

Table 3: Elastic Properties for Alloy 600

Temperature (°F)	Elastic Modulus (x10 ³ ksi)	Mean Thermal Expansion (x10 ⁻⁶ in/in/°F)	Thermal Conductivity (Btu/min-in-°F)	Specific Heat (Btu/lb-°F)
70	31.0	6.8	0.0119	0.108
500	29.0	7.6	0.0147	0.120
700	28.2	7.9	0.0161	0.125
1100	25.9	8.4	0.0192	0.139
1500	23.1	9.0	0.0222	0.148
2500	0.1	10.0	0.0306	0.177
2500.1	N/A	0.0	N/A	N/A

Density (ρ) = 0.30 lb/in³, assumed temperature independent.

Poisson's Ratio (ν) = 0.29, assumed temperature independent.

Table 4: Elastic Properties for Alloy 82/182

Temperature (°F)	Elastic Modulus (x10 ³ ksi)	Mean Thermal Expansion (x10 ⁻⁶ in/in/°F)	Thermal Conductivity (Btu/min-in-°F)	Specific Heat (Btu/lb-°F)
70	31.0	6.8	0.0119	0.108
500	29.0	7.6	0.0147	0.120
700	28.2	7.9	0.0161	0.125
1100	25.9	8.4	0.0192	0.139
1500	23.1	9.0	0.0222	0.148
2500	0.1	10.0	0.0306	0.177
2500.1	N/A	0.0	N/A	N/A

Density (ρ) = 0.30 lb/in³, assumed temperature independent.

Poisson's Ratio (ν) = 0.29, assumed temperature independent.

Table 5: Stress-Strain Data for SA-516 Grade 70 ($\leq 4''$ Thick)

Temperature (°F)	Strain (in/in)	Stress (ksi)
70	0.00128814	38.000
	0.00187809	42.000
	0.00257329	46.000
	0.00381110	50.000
	0.00600383	54.000
500	0.00113553	31.000
	0.00142679	35.875
	0.00183954	40.750
	0.00261139	45.625
	0.00415246	50.500
700	0.00106667	27.200
	0.00132412	32.550
	0.00166876	37.900
	0.00228121	43.250
	0.00354341	48.600
1100	0.00116667	21.000
	0.05116163	22.125
	0.05915444	23.250
	0.06794123	24.375
	0.07755935	25.500
1500	0.00300000	15.000
	0.16717493	15.125
	0.16992011	15.250
	0.17268761	15.375
	0.17547742	15.500
2500	0.01000000	1.000
	0.10961239	1.125
	0.12781277	1.250
	0.14689940	1.375
	0.16683167	1.500

Table 6 Stress-Strain Data for ER308L

Temperature (°F)	Strain (in/in)	Stress (ksi)
70	0.00203180	57.500
	0.02471351	61.563
	0.03107296	65.625
	0.03861377	69.688
	0.04747167	73.750
500	0.00140089	36.143
	0.00714793	40.250
	0.01065407	44.357
	0.01558289	48.464
	0.02233857	52.571
700	0.00132488	32.857
	0.00477547	37.125
	0.00743595	41.393
	0.01143777	45.661
	0.01727192	49.929
1100	0.00121913	26.943
	0.00264833	30.138
	0.00404100	33.332
	0.00634529	36.527
	0.01005286	39.721
1500	0.00117995	21.357
	0.05352064	21.563
	0.05610492	21.768
	0.05878975	21.973
	0.06157807	22.179
2500	0.01000000	1.000
	0.10961239	1.125
	0.12781277	1.250
	0.14689940	1.375
	0.16683167	1.500

Table 7: Stress-Strain Data for Alloy 600

Temperature (°F)	Strain (in/in)	Stress (ksi)
70	0.00157419	48.800
	0.01658847	55.300
	0.02343324	61.800
	0.03212188	68.300
	0.04291703	74.800
500	0.00152069	44.100
	0.01539220	50.338
	0.02210610	56.575
	0.03072476	62.813
	0.04153277	69.050
700	0.00152128	42.900
	0.01634485	49.000
	0.02334760	55.100
	0.03227153	61.200
	0.04338643	67.300
1100	0.00155985	40.400
	0.02275193	44.475
	0.03004563	48.550
	0.03888203	52.625
	0.04943592	56.700
1500	0.00092641	21.400
	0.08827666	22.475
	0.09785101	23.550
	0.10796967	24.625
	0.11863796	25.700
2500	0.01000000	1.000
	0.10961239	1.125
	0.12781277	1.250
	0.14689940	1.375
	0.16683167	1.500

Table 8: Stress-Strain Data for Alloy 182

Temperature (°F)	Strain (in/in)	Stress (ksi)
70	0.00179032	55.500
	0.03456710	60.113
	0.04292837	64.725
	0.05257245	69.338
	0.06359421	73.950
500	0.00164483	47.700
	0.02976152	52.313
	0.03809895	56.925
	0.04790379	61.538
	0.05929946	66.150
700	0.00159574	45.000
	0.02849157	49.538
	0.03680454	54.075
	0.04663682	58.613
	0.05812078	63.150
1100	0.00159073	41.200
	0.03568855	44.488
	0.04402702	47.775
	0.05360088	51.063
	0.06449835	54.350
1500	0.00106494	24.600
	0.11812735	25.325
	0.12540227	26.050
	0.13290814	26.775
	0.14064577	27.500
2500	0.01000000	1.000
	0.10961239	1.125
	0.12781277	1.250
	0.14689940	1.375
	0.16683167	1.500

Table 9: Creep Properties

Material	Temperature (°F)	Creep Strength (ksi)		A (ksi/hr)	n
		σ_1 (0.0001%/hr)	σ_2 (0.00001%/hr)		
SA-516 Gr. 70 (Based on carbon steel)	800	19.0 [6]	12.4 [6]	1.26E-13	5.40
	900	9.0 [6]	6.7 [6]	3.59E-14	7.80
	1000	3.5 [6]	2.8 [6]	2.43E-12	10.32
	1100	1.4 [6]	0.8 [6]	2.50E-07	4.11
ER308L (Based on Type 304)	800	33.4 [6]	25.0 [6]	7.73E-19	7.95
	900	24.0 [6]	17.6 [6]	5.67E-17	7.42
	1000	17.6 [6]	11.5 [6]	1.82E-13	5.41
	1100	11.5 [6]	7.1 [6]	8.62E-12	4.78
Alloy 600 Alloy 82/182 (Based on Alloy 600)	800	40.0 [7]	30.0 [7]	1.50E-19	8.00
	900	28.0 [7]	18.0 [7]	2.87E-14	5.21
	1000	12.5 [7]	6.1 [7]	3.02E-10	3.21
	1100	6.8 [7]	3.4 [7]	1.72E-09	3.32

For Information Only

Table 10: Circumferential Crack “K vs. a” Table

Azimuth (degree)	K (ksi-in ^{0.5}) for Various Crack Depths (inch)						
	0.13	0.57	1.21	1.85	2.49	3.13	3.95
0	17.68	23.56	19.57	9.85	9.20	4.66	20.06
5	17.93	24.48	20.45	10.44	9.68	4.95	20.94
10	17.67	24.46	20.71	10.84	10.06	5.28	21.39
15	17.62	24.44	20.93	11.28	10.49	5.66	21.93
20	17.57	24.33	20.91	11.59	10.81	6.00	22.40
25	17.64	24.27	20.83	11.88	11.12	6.37	22.99
30	17.49	23.77	20.43	12.03	11.32	6.70	23.34
35	17.63	24.25	20.92	12.79	12.02	7.37	24.64
40	17.54	24.36	21.16	13.46	12.67	8.05	25.75
45	17.54	24.49	21.48	14.22	13.38	8.79	26.93
50	17.56	24.67	21.86	15.00	14.10	9.54	28.14
55	17.48	24.89	22.22	15.72	14.77	10.24	29.34
60	17.65	25.62	22.99	16.66	15.63	11.05	31.03
65	17.52	25.32	22.91	16.89	15.85	11.37	31.67
70	17.59	25.43	23.21	17.35	16.27	11.79	32.62
75	17.58	25.50	23.51	17.80	16.66	12.19	33.38
80	17.62	25.69	23.91	18.33	17.12	12.61	34.10
85	17.48	25.85	24.19	18.73	17.48	12.91	34.54
90	17.78	26.93	25.14	19.58	18.22	13.47	35.74

Notes:

1. The 0° azimuth is at the axial cut plane of the hot leg (see Figure 1).
2. The 90° azimuth is at the circumferential cut plane of the hot leg (see Figure 1).

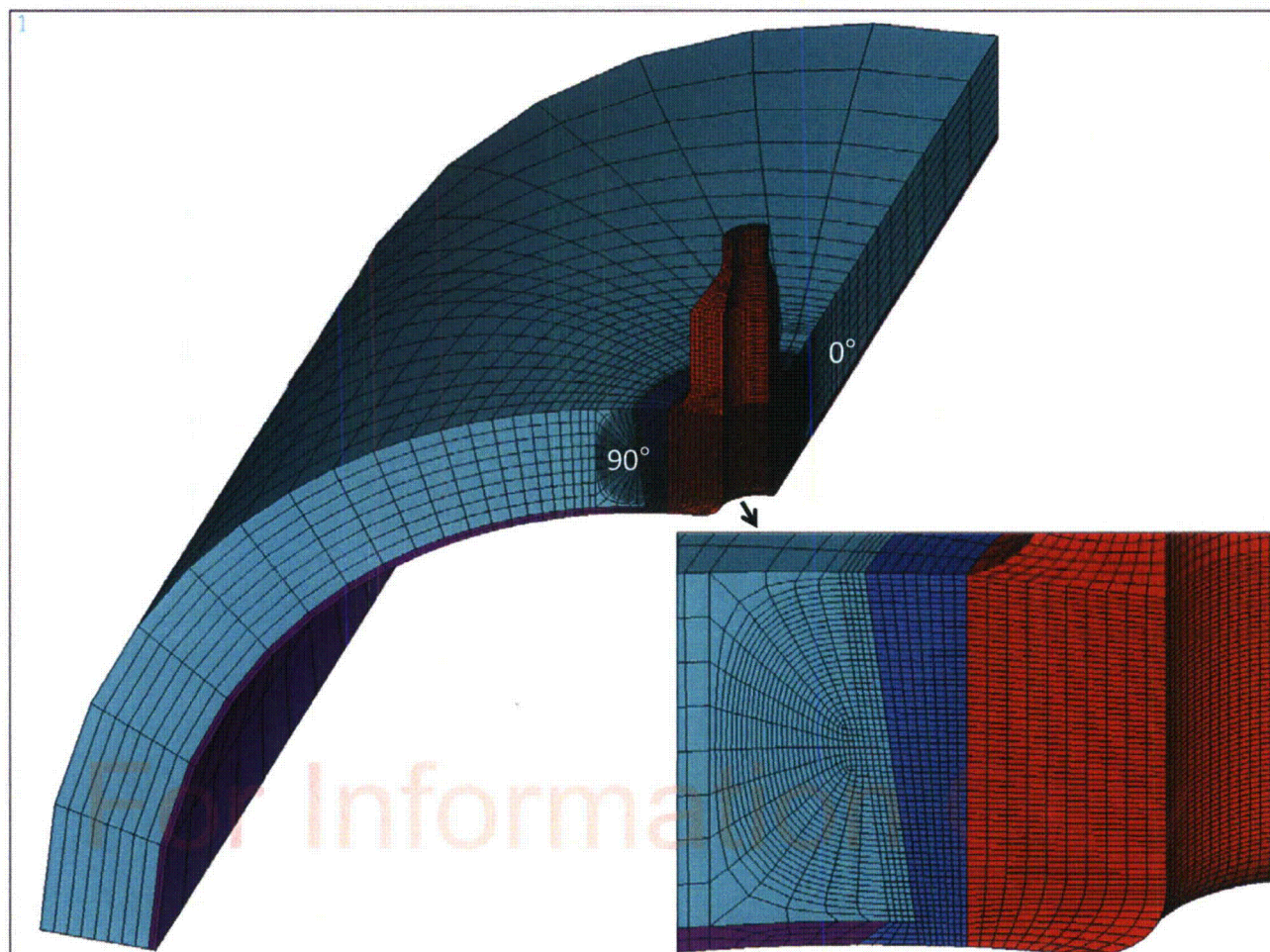


Figure 1: Finite Element Model for Residual Stress Analysis

Notes:

1. The 0° azimuth is at the axial cut plane of the hot leg.
2. The 90° azimuth is at the circumferential cut plane of the hot leg.

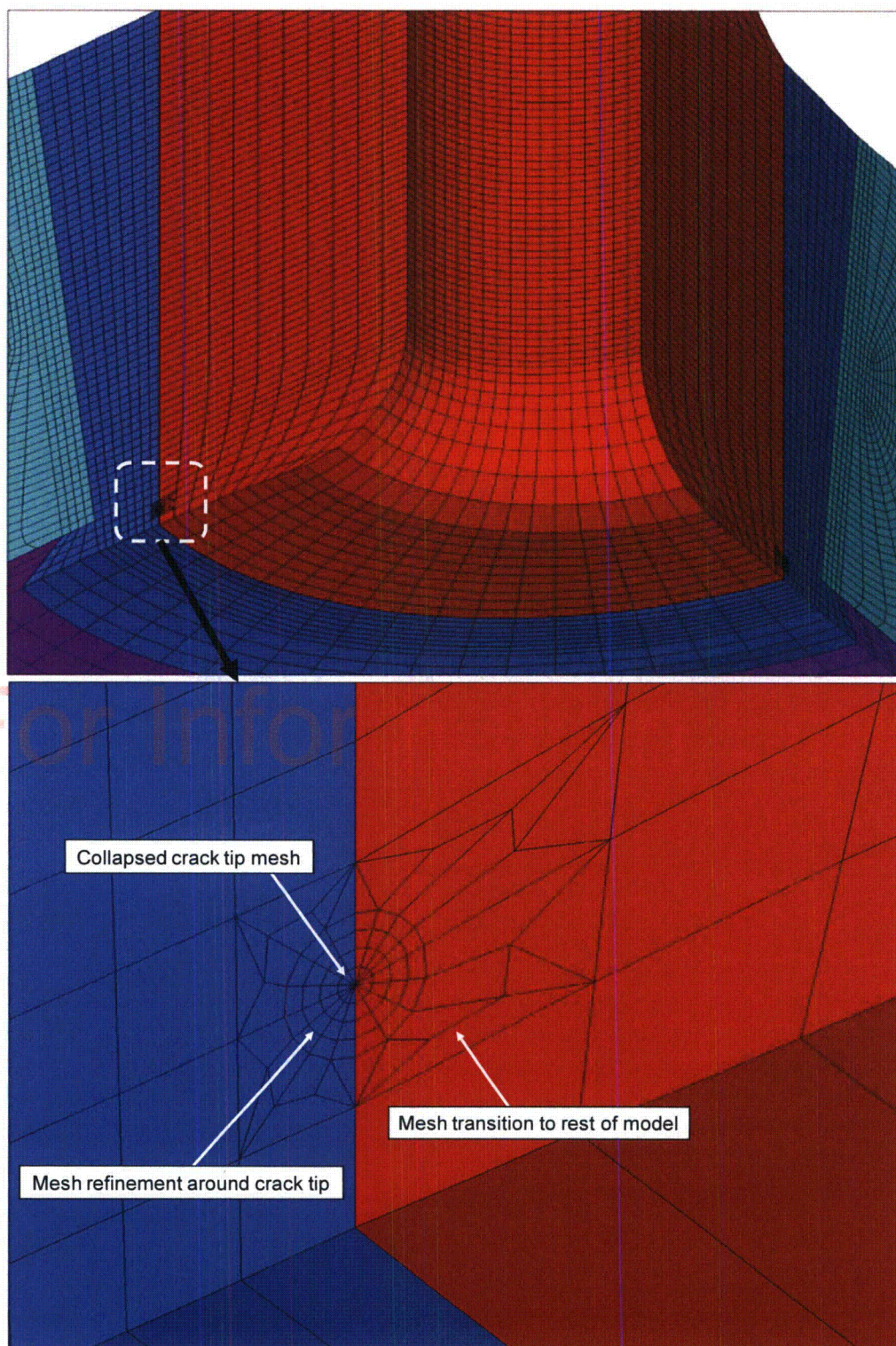


Figure 2: Finite Element Model for the 0.13" Deep Circumferential Crack

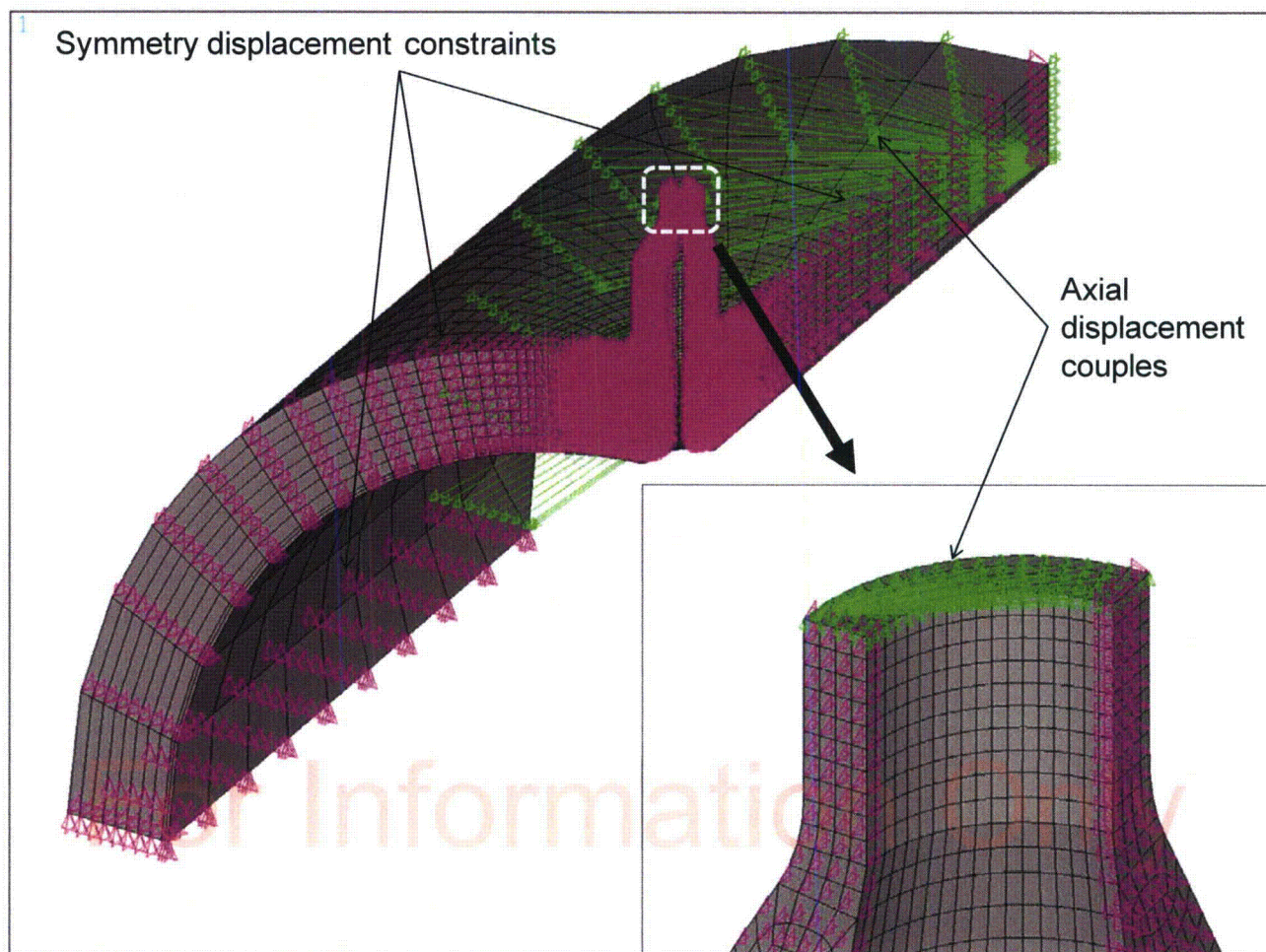


Figure 3: Applied Mechanical Boundary Conditions

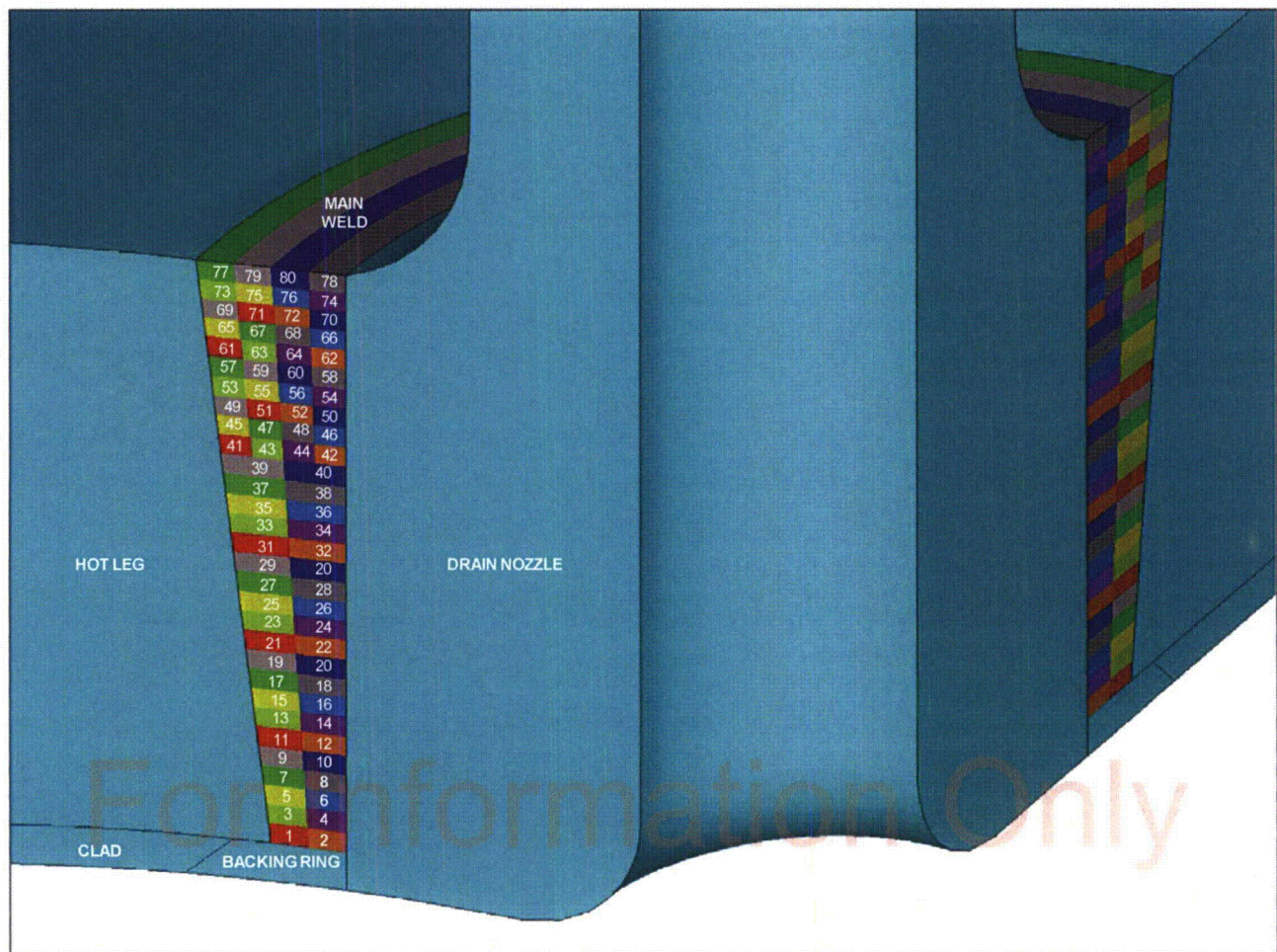


Figure 4: Weld Nugget Definitions for the Boss Main Weld

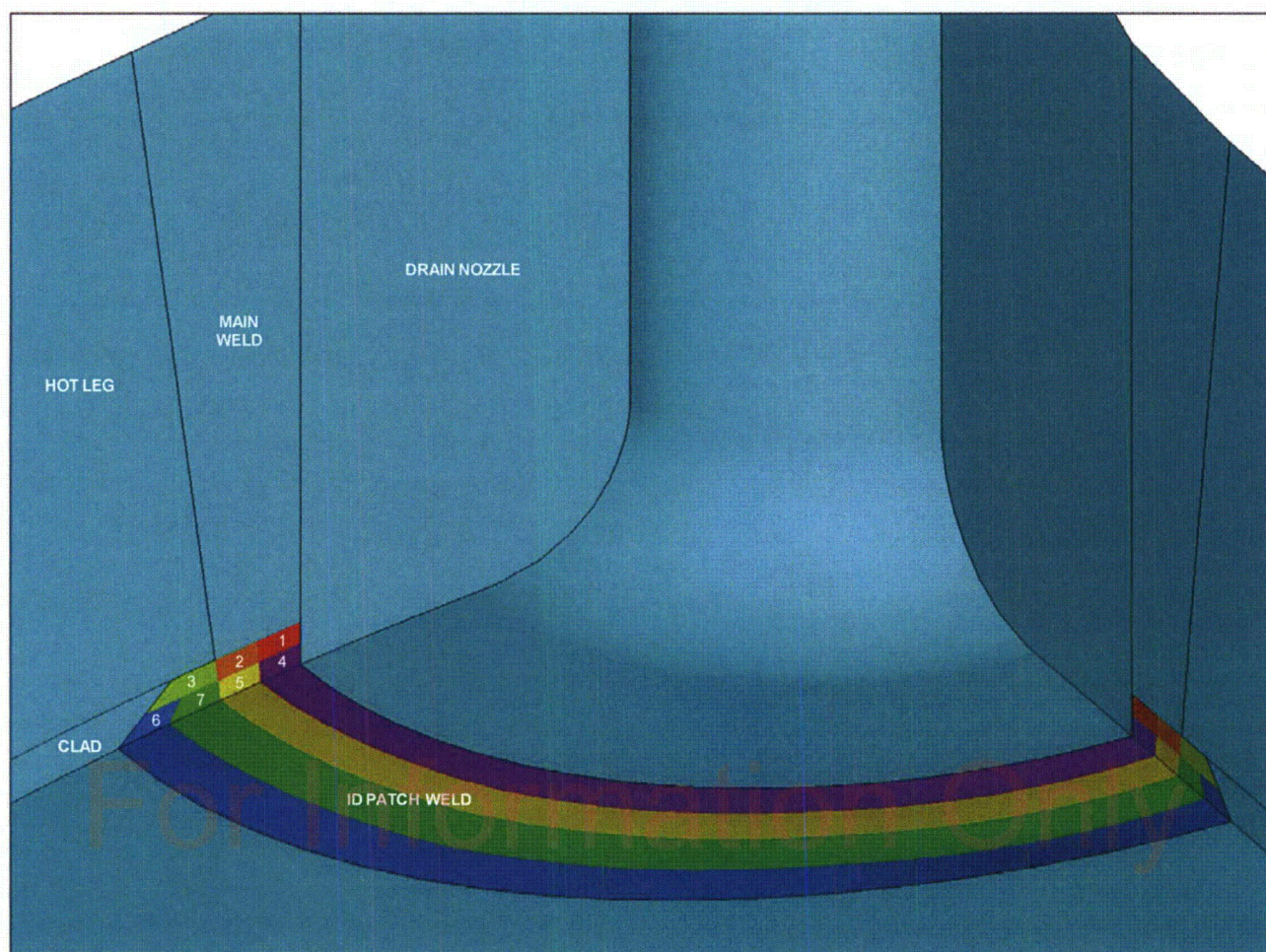


Figure 5: Weld Nugget Definitions for the ID Patch Weld

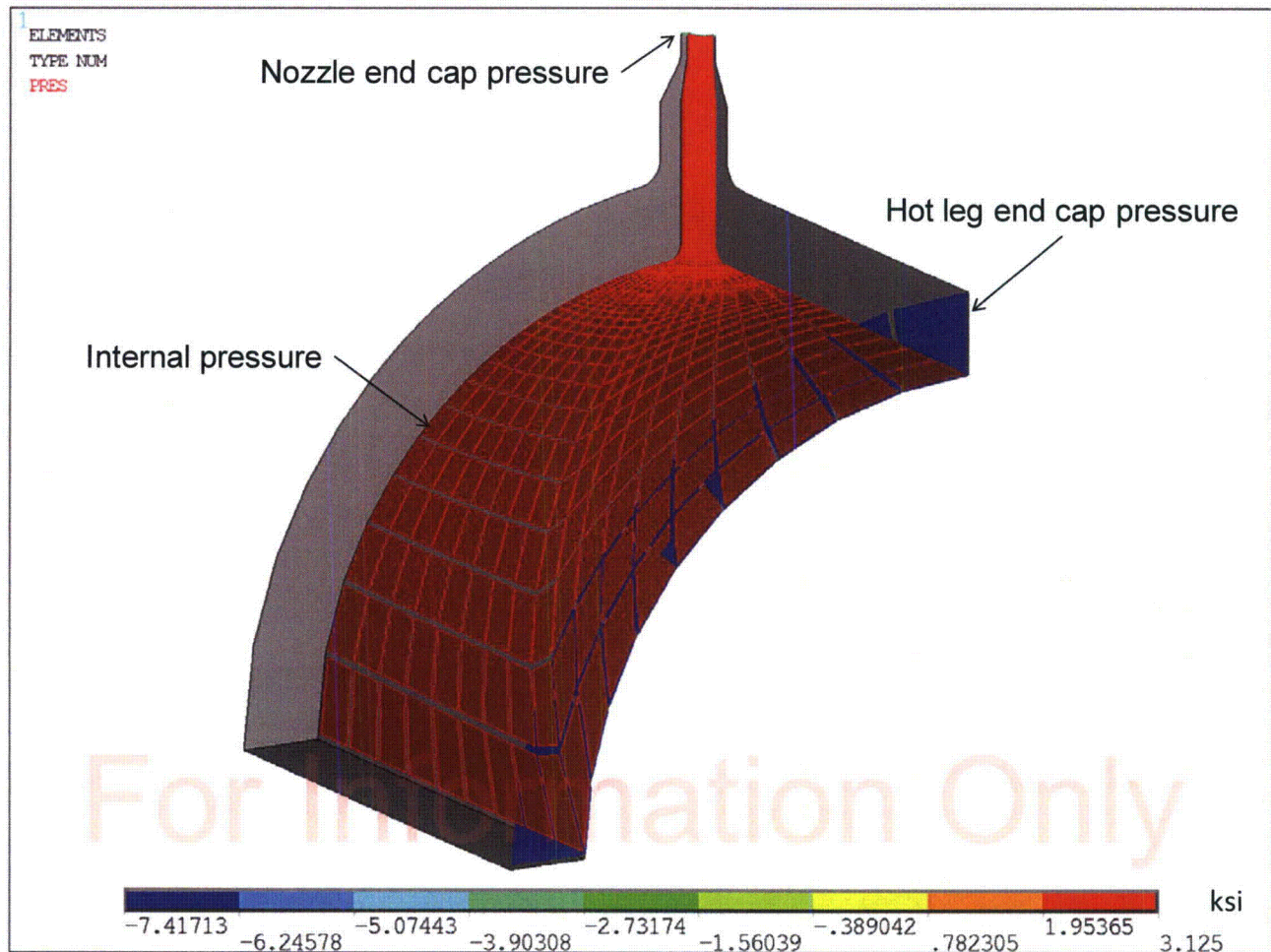


Figure 6: Applied Hydrostatic and Corresponding End Cap Pressure Loads

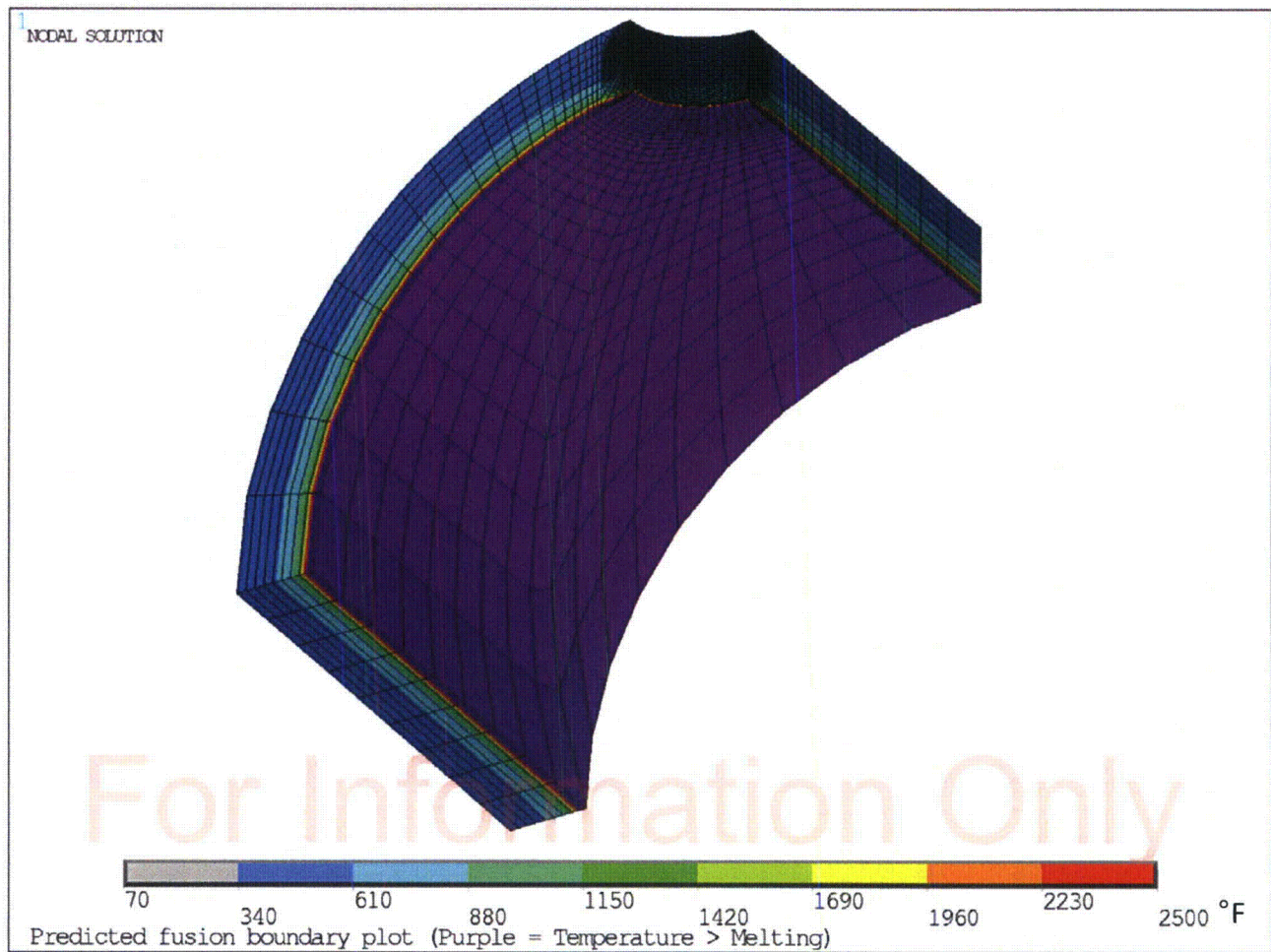


Figure 7: Predicted Fusion Boundary Plot for Cladding

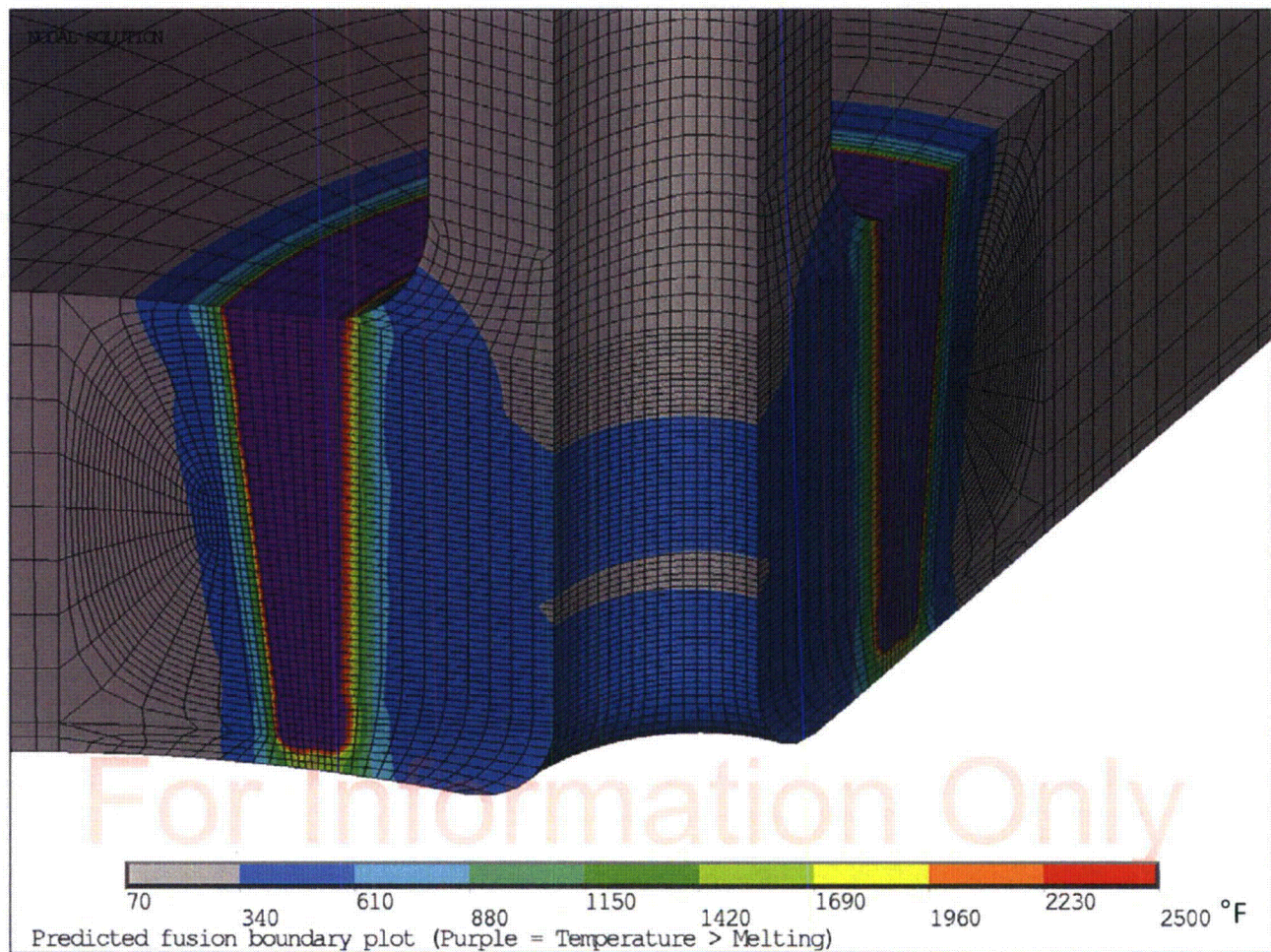


Figure 8: Predicted Fusion Boundary Plot for Boss Main Weld

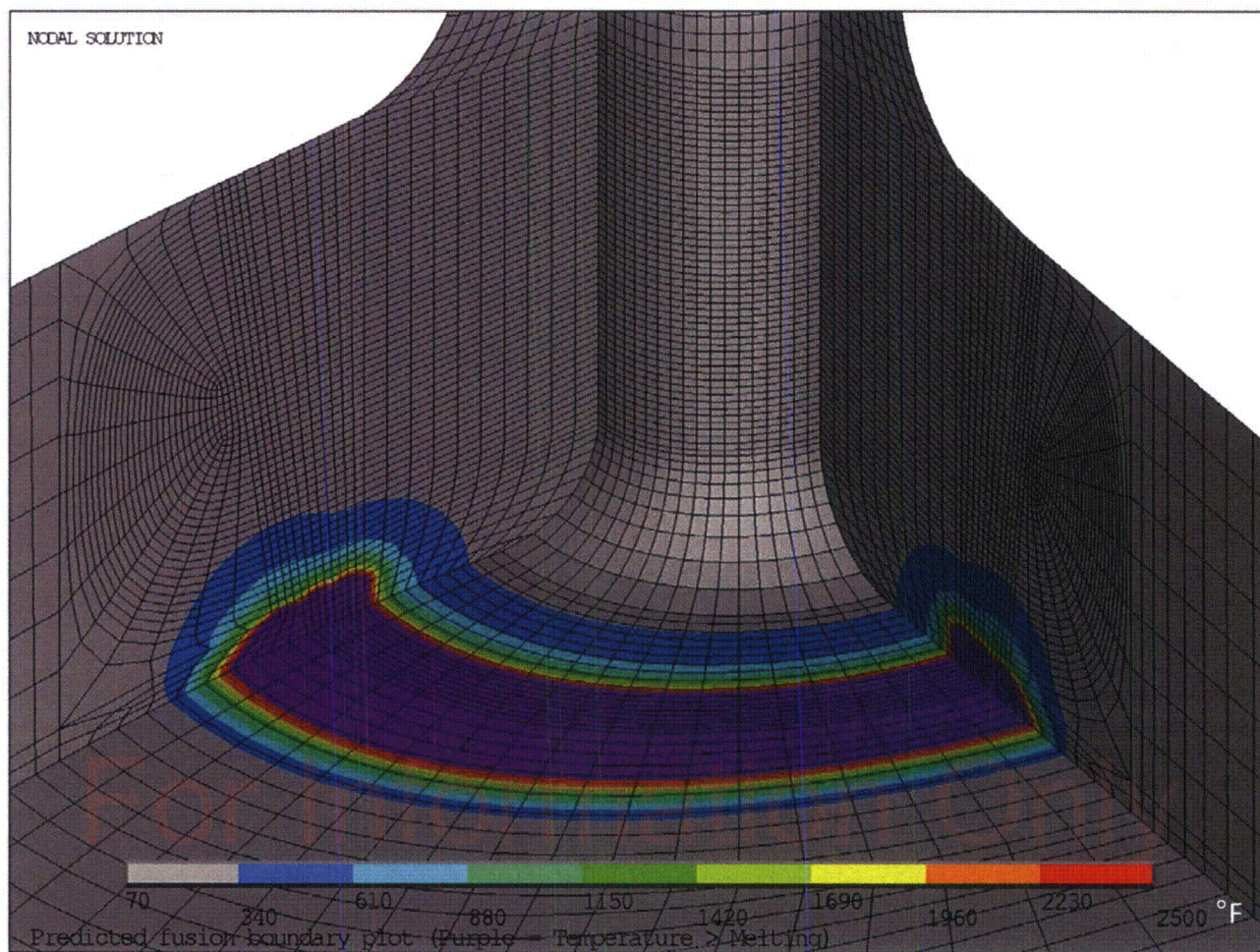


Figure 9: Predicted Fusion Boundary Plot for ID Patch Weld

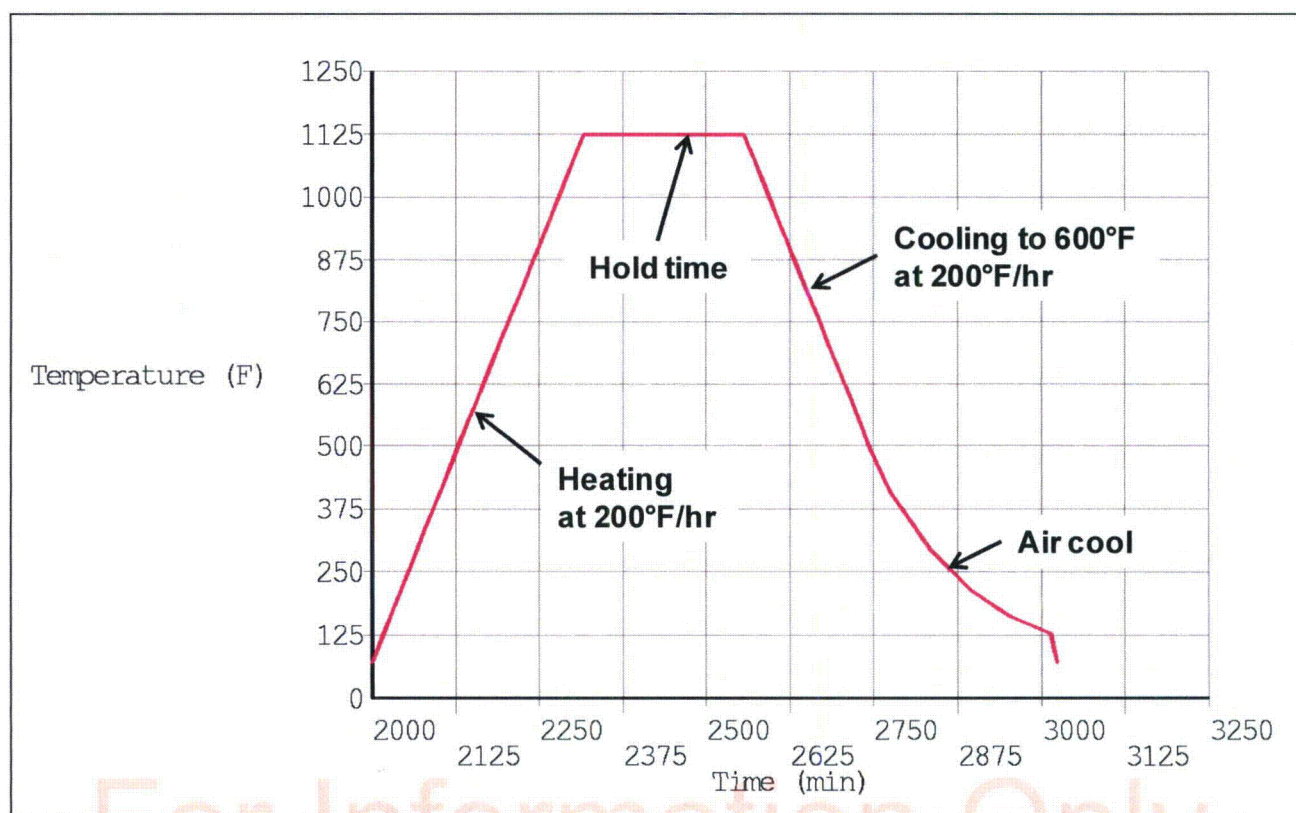


Figure 10: Temperature Curve for PWHT

Note:

1. PWHT temperature history is for an arbitrary ID node on the model.

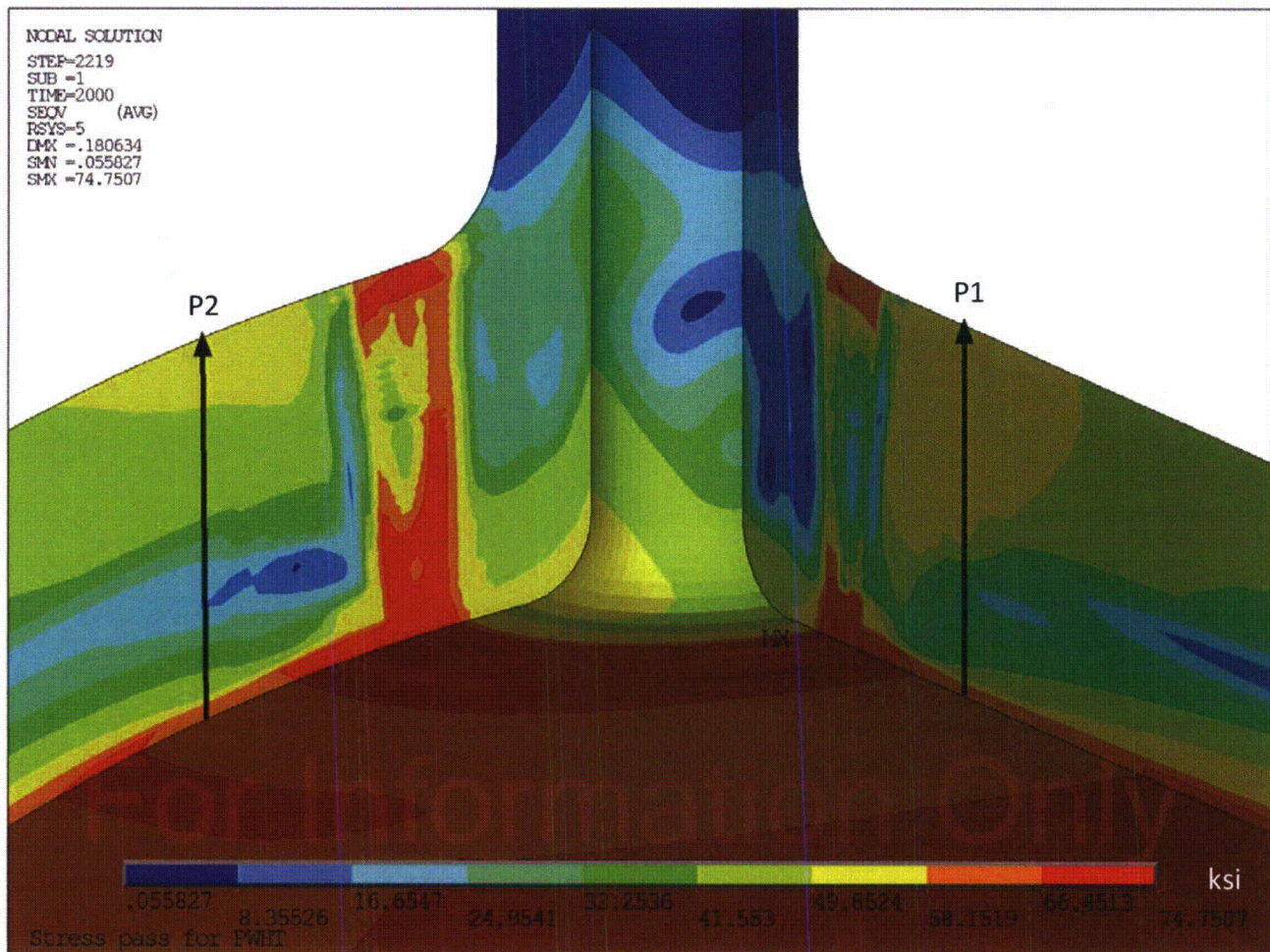


Figure 11: Predicted von Mises Residual Stress after ID Patch Weld at 70°F

Notes:

1. In the hot leg coordinates, hoop residual stresses along path P1 and axial residual stresses along path P2 are extracted for before and after PWHT.
2. The before and after PWHT through-wall residual stresses are compared in Figure 13.

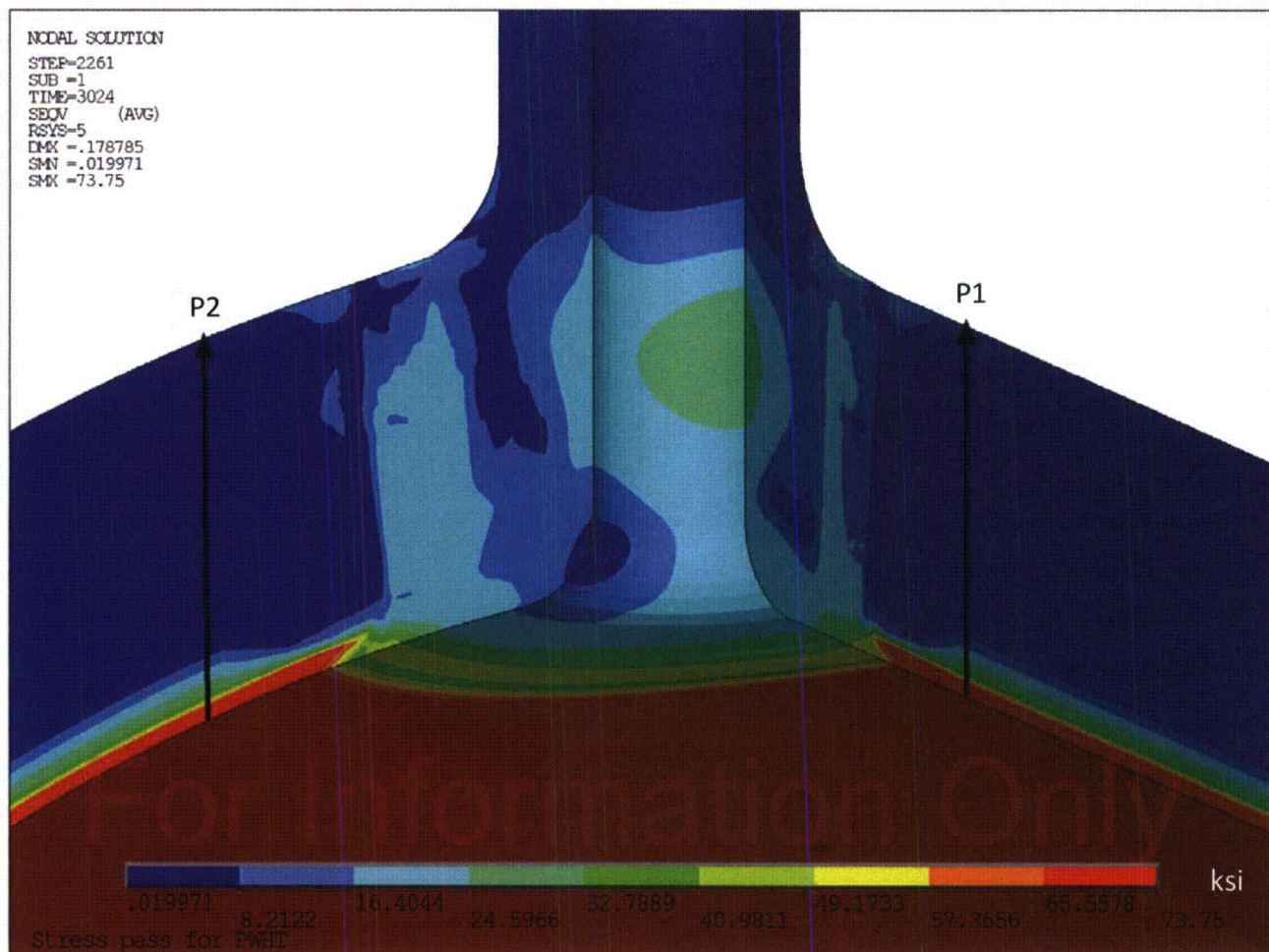


Figure 12: Predicted von Mises Residual Stress after PWHT at 70°F

Notes:

1. In the hot leg coordinates, hoop residual stresses along path P1 and axial residual stresses along path P2 are extracted for before and after PWHT.
2. The before and after PWHT through-wall residual stresses are compared in Figure 13.

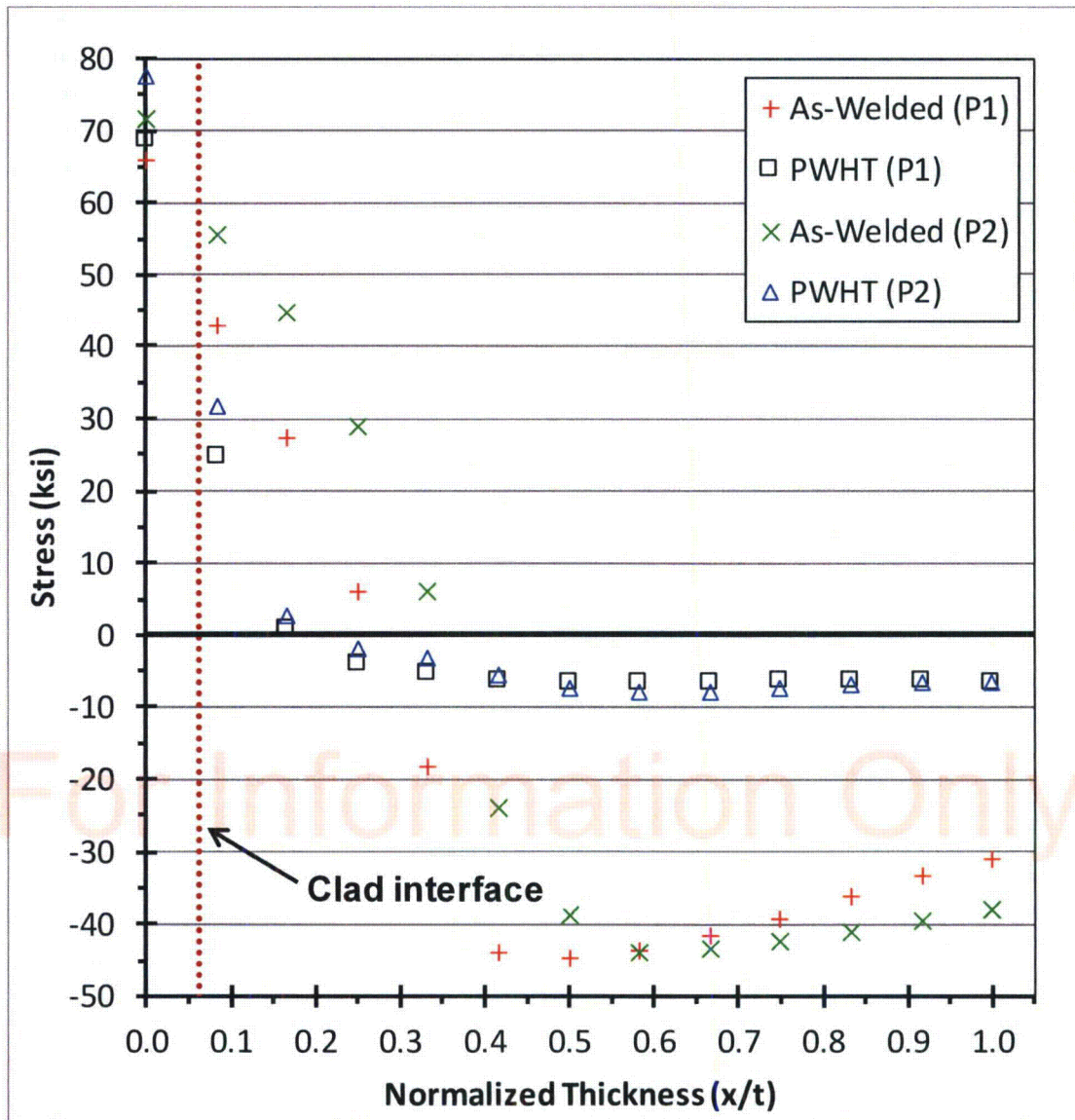


Figure 13: Residual Stress Comparison for Before and After PWHT

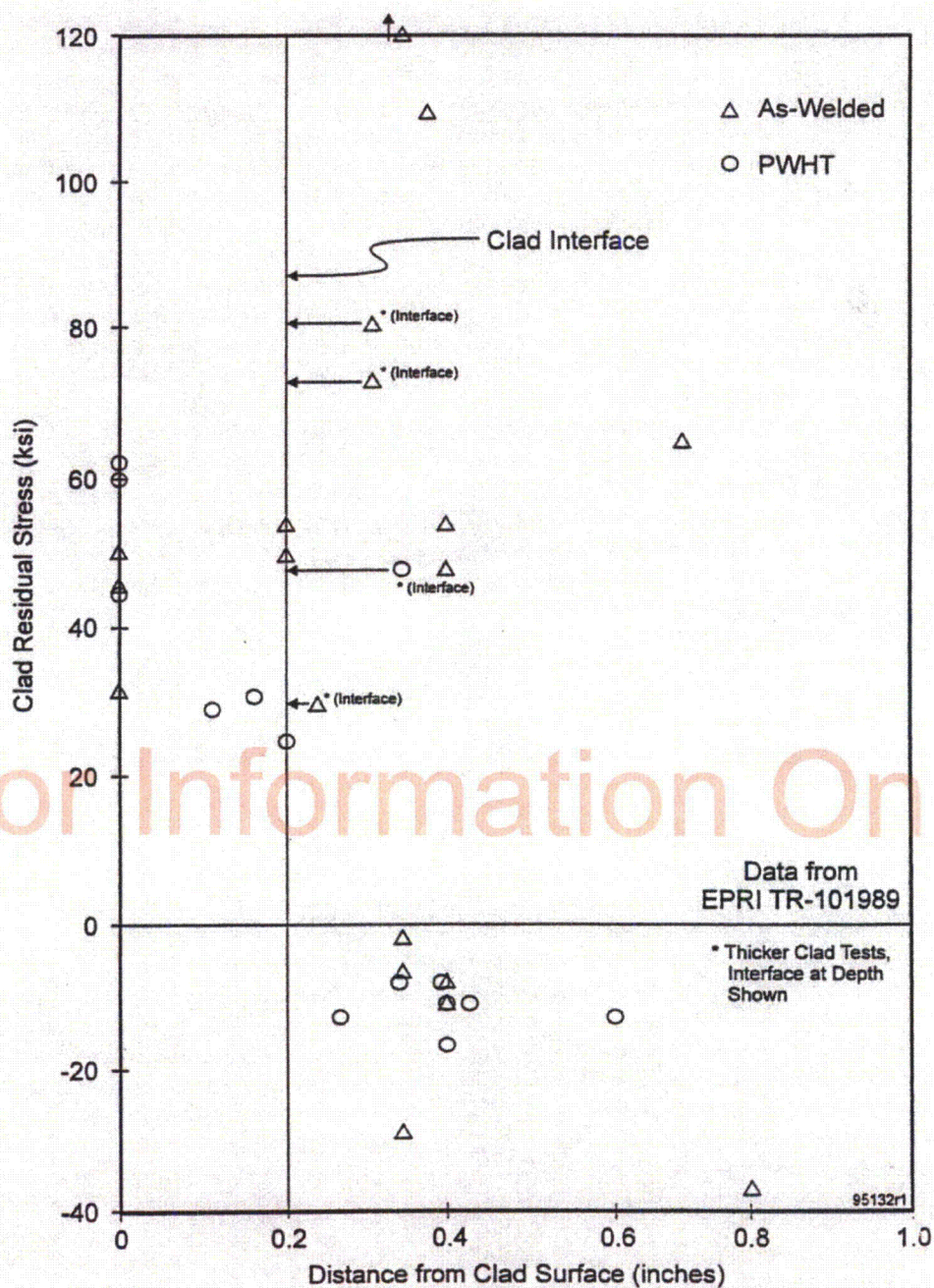


Figure 14: Measured Through-Wall Residual Stresses for PWHT

Notes:

1. Figure is obtained from EPRI report TR-105697 [12].
2. Measurements show little to no stress reduction in the cladding after PWHT.
3. Measurements show significant stress reduction in the base metal after PWHT.

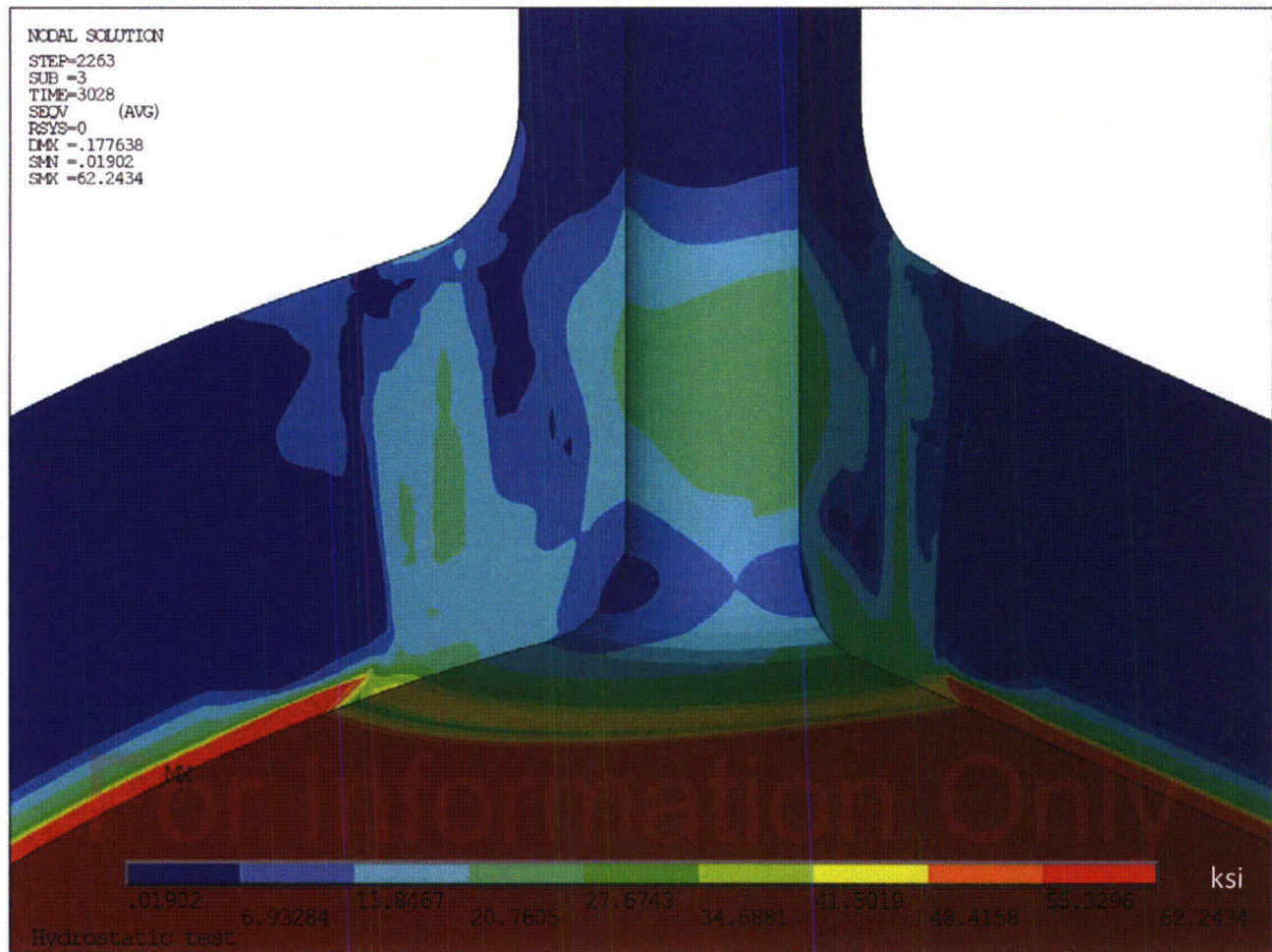


Figure 15: Predicted von Mises Residual Stress after Hydrostatic Test at 70°F

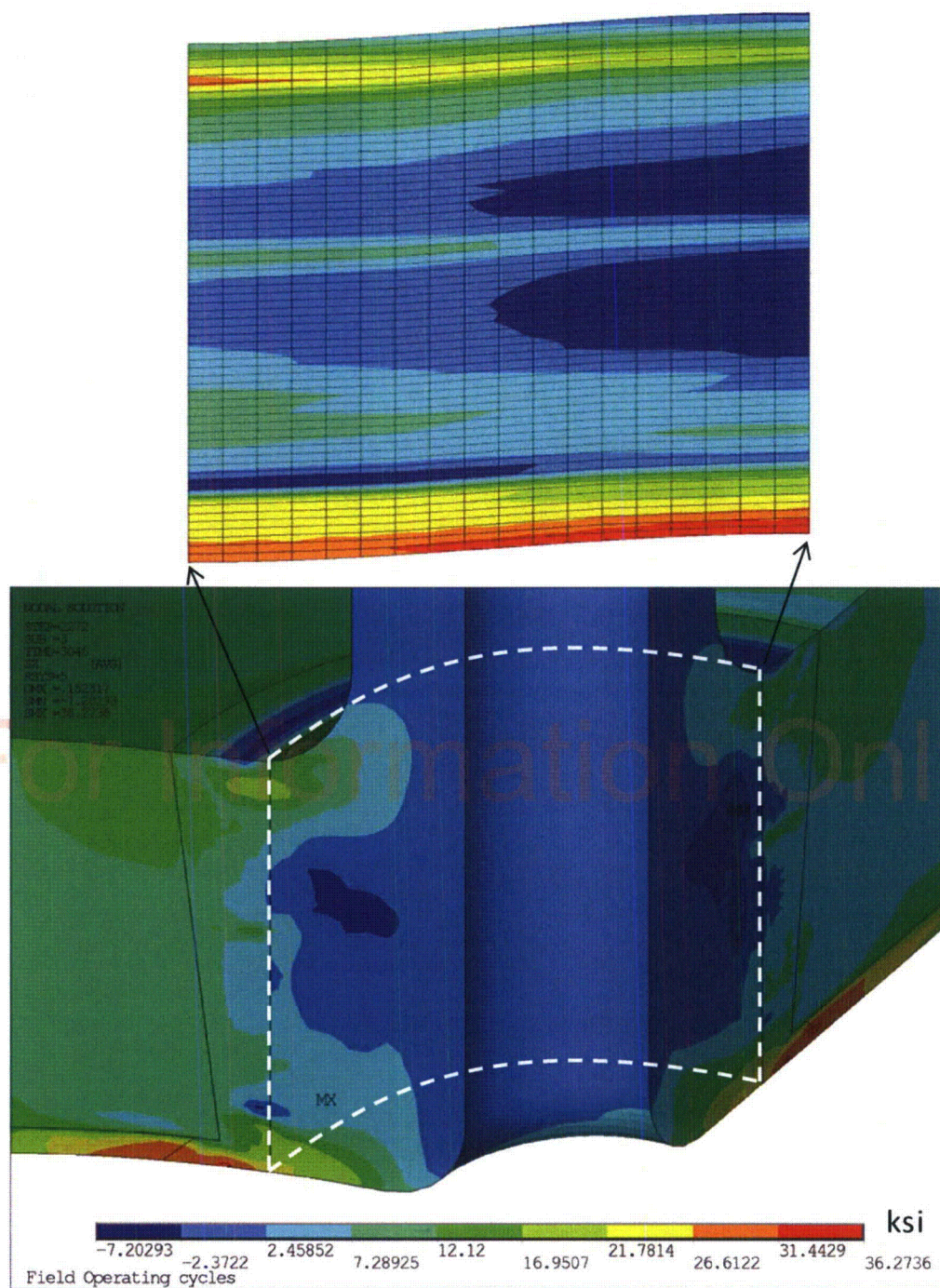


Figure 16: Predicted Radial Residual Stress + Operating Conditions (5th NOC Cycle)

Note:

1. Radial stresses in the nozzle axis.

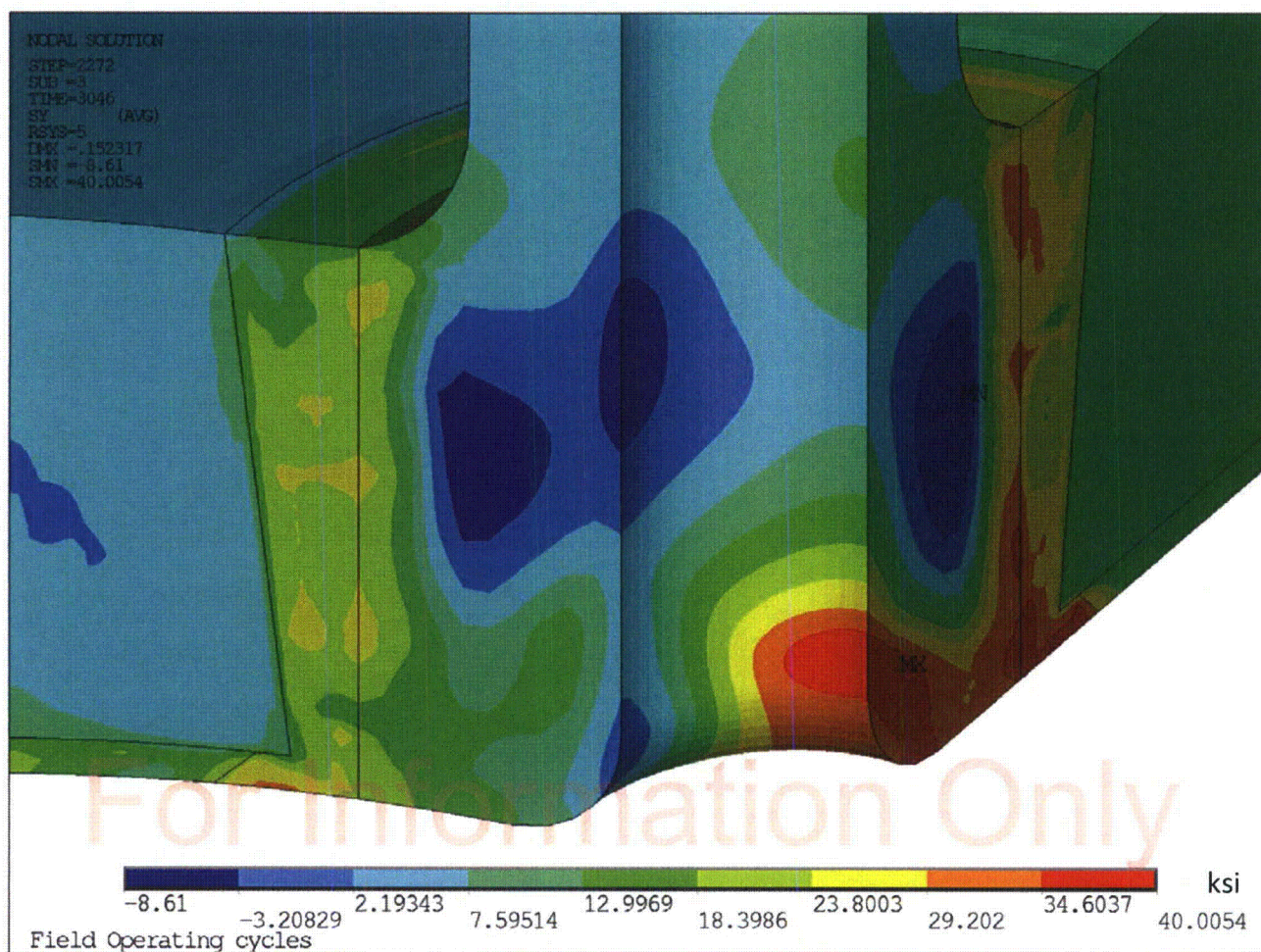


Figure 17: Predicted Hoop Residual Stresses + Operating Conditions (5th NOC Cycle)

Note:

1. Hoop stresses in the nozzle axis.

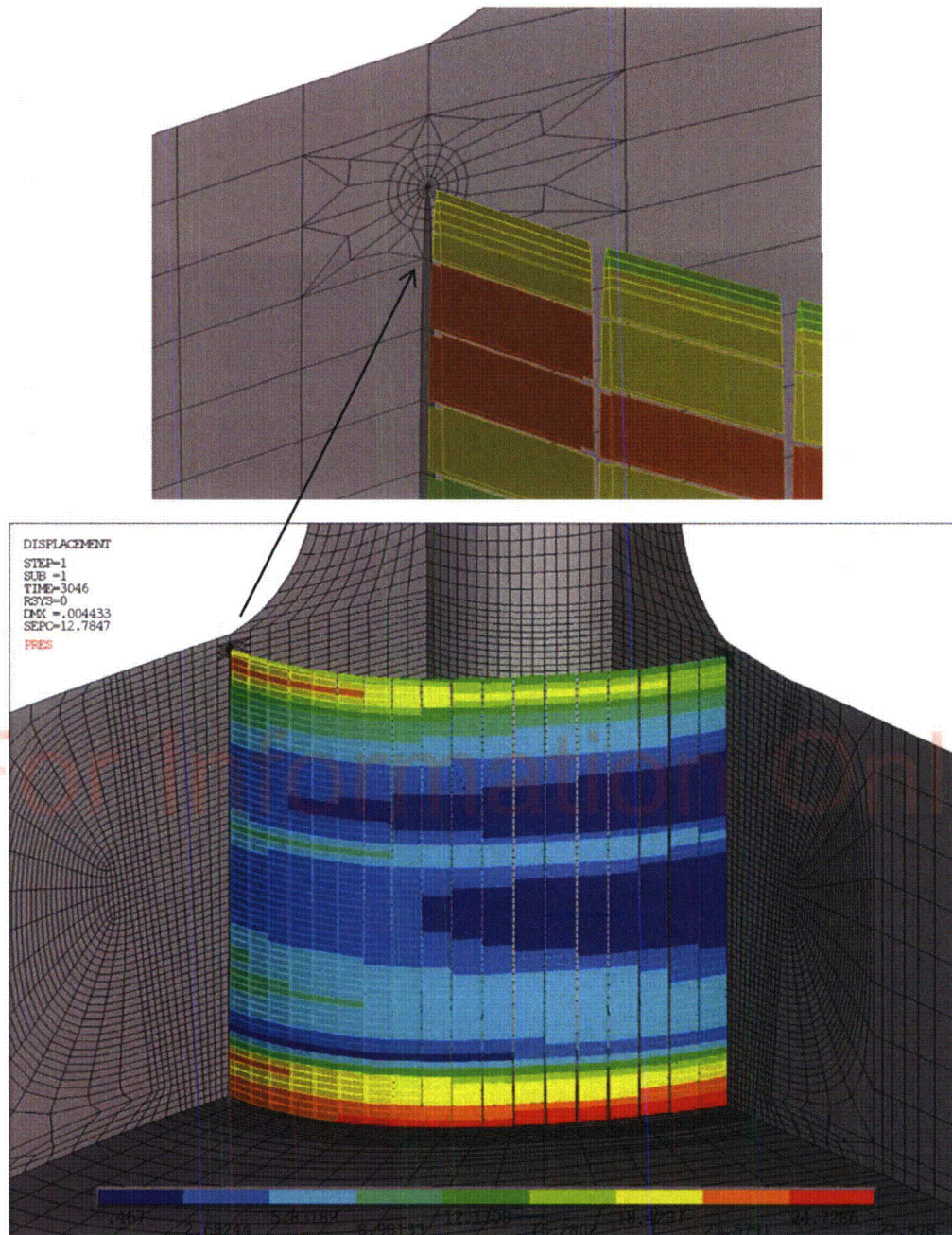


Figure 18: Transferred Radial Residual + NOC + Pressure Stresses (3.95" Crack Shown)

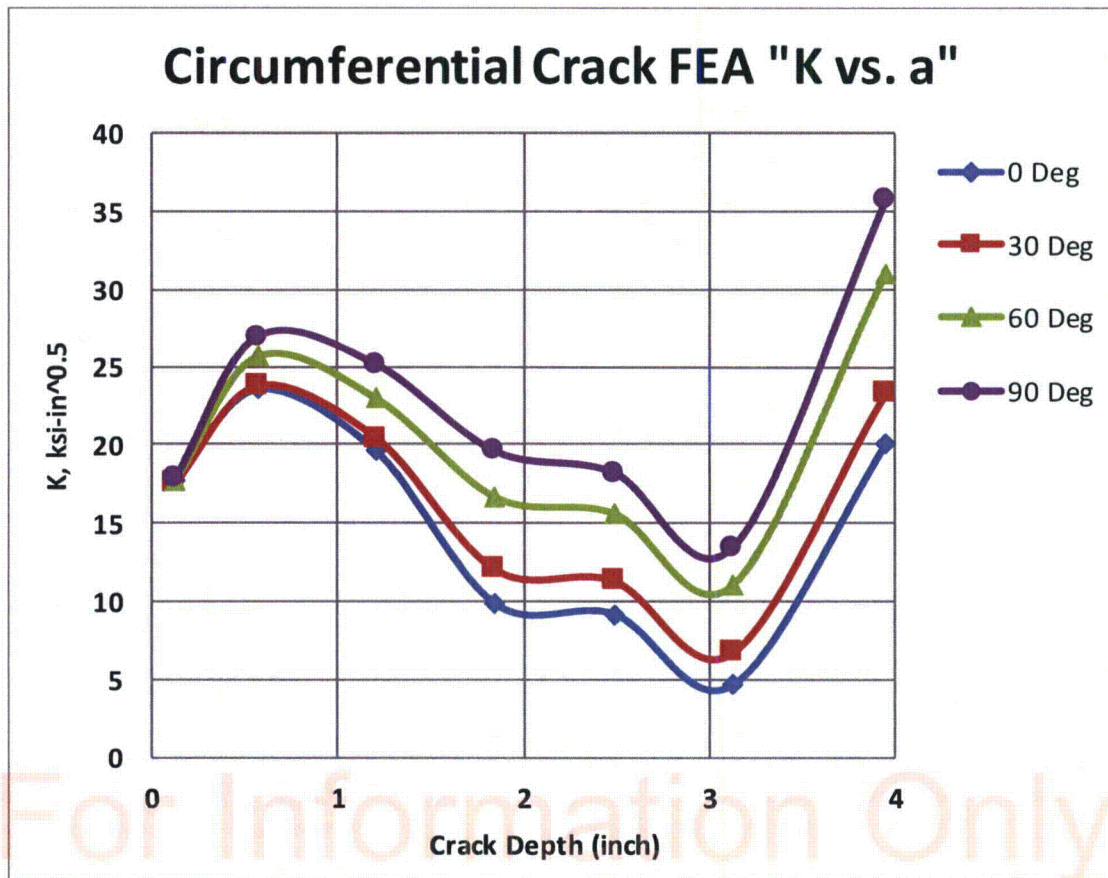


Figure 19: FEA Calculated Circumferential Crack "K vs. a" at Four Azimuth Locations

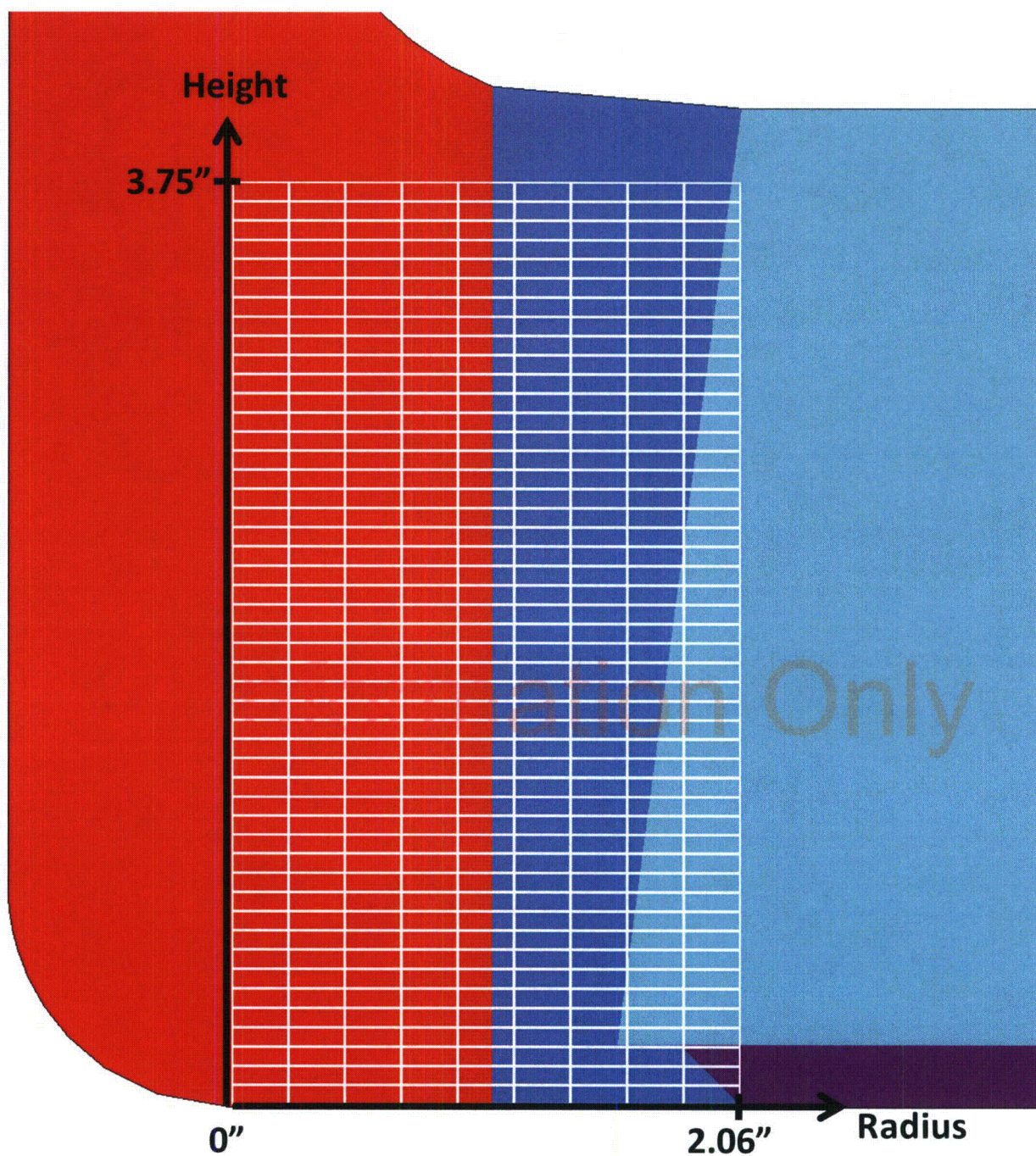


Figure 20: Hoop Stress Extraction Grid for Axial Crack Growth Evaluation